BAMS Article

Dust, Convection, Winds, and Waves: The 2022 NASA CPEX-CV Campaign

Edward P. Nowottnick,[a] Angela K. Rowe,[b] Amin R. Nehrir,[c] Jonathan A. Zawislak,[d] Aaron J. Piña,[e,f] Will McCarty,[g] Rory A. Barton-Grimley,[c] Kristopher M. Bedka,[c] J. Ryan Bennett,[h] Alan Brammer,[i] Megan E. Buzanowicz,[j,c] Gao Chen,[c] Shu-Hua Chen,[k] Shuyi S. Chen,[l] Peter R. Colarco,[a] John W. Cooney,[c] Ewan Crosbie,[m,c] James Doyle,[n] Thorsten Fehr,[o] Richard A. Ferrare,[c] Steven D. Harrah,[c] Svetla M. Hristova-Veleva,[p] Bjorn H. Lambrigtsen,[p] Quinton A. Lawton,[q] Allan Lee,[k] Eleni Marinou,[r] Elinor R. Martin,[s] Griša Močnik,[t,u] Edoardo Mazza,[v] Raquel Rodriguez Monje,[p] Kelly M. Núñez Ocasio,[w,x] Zhaoxia Pu,[y] Manikandan Rajagopal,[y] Jeffrey S. Reid,[n] Claire E. Robinson, Rosimar Rios-Berrios,[w] Benjamin D. Rodenkirch,[b] Naoko Sakaeda,[s] Vidal Salazar,[z] Michael A. Shook,[c] Leigh Sinclair,[aa] Gail M. Skofronick-Jackson, K. Lee Thornhill,[m,c] Ryan D. Torn,[bb] David P. Van Gilst,[h] Peter G. Veals,[y] Holger Vömel,[w] Sun Wong,[p] Shun-Nan Wu,[s] Luke D. Ziemba,[c] and Edward J. Zipser[y]

KEYWORDS: Convective-scale processes; Data assimilation; Aerosols/ particulates

ABSTRACT: The NASA Convective Processes Experiment-Cabo Verde (CPEX-CV) field campaign took place in September 2022 out of Sal Island, Cabo Verde. A unique payload aboard the NASA DC-8 aircraft equipped with advanced remote sensing and in situ instrumentation, in conjunction with radiosonde launches and satellite observations, allowed CPEX-CV to target the coupling between atmospheric dynamics, marine boundary layer properties, convection, and the dust-laden Saharan air layer in the data-sparse tropical East Atlantic region. CPEX-CV provided measurements of African easterly wave environments, diurnal cycle impacts on convective life cycle, and several Saharan dust outbreaks, including the highest dust optical depth observed by the DC-8 interacting with what would become Tropical Storm Hermine. Preliminary results from CPEX-CV underscore the positive impact of dedicated tropical East Atlantic observations on downstream forecast skill, including sampling environmental forcings impacting the development of several nondeveloping and developing convective systems such as Hurricanes Fiona and Ian. Combined airborne radar, lidar, and radiometer measurements uniquely provide near-storm environments associated with convection on various spatiotemporal scales and, with in situ observations, insights into controls on Saharan dust properties with transport. The DC-8 also collaborated with the European Space Agency to perform coordinated validation flights under the Aeolus spaceborne wind lidar and over the Mindelo ground site, highlighting the enhanced sampling potential through partnership opportunities. CPEX-CV engaged in professional development through dedicated team-building exercises that equipped the team with a cohesive approach for targeting CPEX-CV science objectives and promoted active participation of scientists across all career stages.

DOI: 10.1175/BAMS-D-23-0201.1
Corresponding author: Edward P. Nowottnick, edward.p.nowottnick@nasa.gov
Supplemental information related to this paper is available at the Journals Online website: https://doi.org/10.1175/BAMS-D-23-0201.s1.

Manuscript received 31 July 2023, in final form 21 August 2024, accepted 30 August 2024

SIGNIFICANCE STATEMENT: Sparse data over the tropical East Atlantic Ocean challenge forecasting of downstream impacts, including hurricane formation and Saharan dust transport. The NASA Convective Processes Experiment-Cabo Verde measured vertical profiles of winds, dust, and moisture near and within clouds and precipitating storms in this region during September 2022 using aircraft outfitted with a unique set of instrumentation. With 13 research flights covering 90 h, analysis of these data shows the positive impact of these observations on forecast skill, highlights the detrimental impacts of dry air on early hurricane development, challenges previous thinking on how dust is vertically distributed in the atmosphere, and connects winds with storm structure and intensity. This dataset is publicly available for further research on these relationships.

AFFILIATIONS: [a] NASA Goddard Space Flight Center, Greenbelt, Maryland; [b] University of Wisconsin–Madison, Madison, Wisconsin; [c] NASA Langley Research Center, Hampton, Virginia; [d] NOAA/Office of Marine and Aviation Operations, Lakeland, Florida; [e] Formerly at NASA Headquarters, Washington, D.C.; [f] U.S. Forest Service, Washington, D.C.; [g] NASA Headquarters, Washington, D.C.; [h] Bay Area Environmental Research Institute, NASA Ames Research Center, Moffett Field, California; [i] Cooperative Institute for Research in the Atmosphere, Colorado State University, Fort Collins, Colorado; [j] ADNET Systems, Inc., Bethesda, Maryland; [k] University of California, Davis, Davis, California; [l] University of Washington, Seattle, Washington; [m] Analytical Mechanics Associates, Hampton, Virginia; [n] U.S. Naval Research Laboratory, Monterey, California; [o] European Space Agency, Noordwijk, Netherlands; [p] Jet Propulsion Laboratory, California Institute of Technology, Pasadena, California; [q] Rosenstiel School of Marine, Atmospheric and Earth Science, University of Miami, Miami, Florida; [r] National Observatory of Athens, Athens, Greece; [s] University of Oklahoma, Norman, Oklahoma; [t] University of Nova Gorica, Nova Gorica, Slovenia; [u] Haze Instruments d.o.o., Ljubljana, Slovenia; [v] NOAA/Pacific Marine Environmental Laboratory, Seattle, Washington; [w] National Science Foundation National Center for Atmospheric Research, Boulder, Colorado; [x] Texas A&M University, College Station, Texas; [y] The University of Utah, Salt Lake City, Utah; [z] NASA Ames Research Center, Moffett Field, California; [aa] University of Alabama-Huntsville, Huntsville, Alabama; [bb] University at Albany, State University of New York, Albany, New York
Robinson and Skofronick-Jackson: Deceased.

1. Introduction

The eastern tropical North Atlantic is the birthplace of some of the most striking atmospheric features on Earth where atmospheric dynamics, convection, and aerosol particles interact as a coupled system. With the arid North African continent to the east, the tropical East Atlantic is subject to Saharan air layer (SAL) outbreaks containing large concentrations of dust originating from the Saharan Desert, the largest source of aerosol on Earth (Ginoux et al. 2012; Textor et al. 2006; Prospero et al. 2002). Dust affects Earth's radiation budget (Mahowald et al. 2014; Zhu et al. 2007; Wong et al. 2009; Chen et al. 2010), cloud structure and lifetimes through influences on cloud microphysics (Kaufman et al. 2005; Rosenfeld et al. 2001; Huang et al. 2019), terrestrial and aquatic life (Jickells et al. 2005; Swap et al. 1992), and air quality (Querol et al. 2019) as far west as the Americas (Yu et al. 2021; Prospero 1999). The dry air associated with SAL also influences the planetary boundary layer structures (Wong et al. 2009) and the development of deep convection (Wong and Dessler 2005). South of the Saharan Desert lies the Sahel where the African easterly jet (AEJ) forms during boreal summer because of the strong zonal thermal gradient between the desert and the cooler waters of the

Gulf of Guinea (Cook 1999; Thorncroft and Blackburn 1999). African easterly waves (AEWs), a frequent occurrence in this region (Burpee 1972), can be generated, maintained, or enhanced by the AEJ (Thorncroft and Hoskins 1994) and embedded mesoscale convective systems (MCSs) (Núñez Ocasio et al. 2020a). These AEWs carry and are modulated by large atmospheric moisture content and are known precursors to Atlantic tropical cyclones (TCs) (Landsea et al. 1998) with implications for the Caribbean and North America (e.g., Thorncroft and Hodges 2001; Burpee 1974). Farther south, near the equator, tropical trade winds converge and form the intertropical convergence zone (ITCZ). Within the ITCZ, deep convection and intense precipitation can result from the ascending component of the Hadley cell (Schneider et al. 2014). During boreal summer in particular, accurate forecasting of these striking features originating from the tropical East Atlantic and their interaction is critical for downstream impacts on human life (Pu and Jin 2021; Rappaport 2014).

Despite serving as a critical region for Atlantic hurricane activity and driving global atmospheric circulation, the tropical East Atlantic, like much of the world's tropical oceans, is sparsely observed. The lack of observations from ground-based networks and limitations from spaceborne vantage points leads to gaps in our understanding of key processes across varying spatiotemporal scales that have significant implications for convective and aerosol life cycles, and consequently forecast skill, downwind. Therefore, observations acquired in the tropical East Atlantic to augment our current ground- and space-based observing systems have an opportunity to significantly affect forecasting skill through data assimilation and improved representation of convective and aerosol processes in global and regional models.

To address the need for higher spatially and temporally resolved data in this region to improve process-level understanding, the National Aeronautics and Space Administration (NASA) Convective Processes Experiment-Cabo Verde (CPEX-CV) field campaign was based in Sal Island, Cabo Verde, on 1–30 September 2022 as the next iteration of the CPEX campaigns, following CPEX 2017 (Turk et al. 2020) and CPEX-Aerosols and Wind (CPEX-AW) (https://espo.nasa.gov/cpex-aw/content/CPEX-AW) field campaigns. With the move to Cabo Verde, CPEX-CV coincidentally observed atmospheric dynamics, marine boundary layer (MBL) properties, convective structure, and the often dust-laden SAL both near and downwind from the African continent. These observations were possible through a unique payload aboard the NASA DC-8 medium-altitude research aircraft, providing simultaneous measurements of tropospheric aerosols, winds, temperature, water vapor, and precipitation interactions in coordination with dedicated ground-based radiosonde launches and collaboration with European partners through the European Space Agency (ESA) coordinated Joint Aeolus Tropical Atlantic Campaign (JATAC).

The international CPEX-CV campaign builds off a history of influential field observations in this region and a broader effort to provide professional development opportunities for scientists and engineers at various stages of their careers. CPEX-CV planning activities included dedicated team-building activities ahead of the deployment and hands-on learning opportunities for early career participants toward training the next generation of flight scientists, instrument scientists, and field campaign leadership.

2. Historical context: 50 years since GATE

Arguably, the largest and most comprehensive field program effort known within the history of the atmospheric sciences targeted the data-sparse eastern tropical Atlantic in 1974: the Global Atmospheric Research Program's Atlantic Tropical Experiment (GATE; Fig. 1). Based out of Dakar, Senegal, GATE included over 5000 participants from 72 countries, 13 aircraft, 39 ships, and over 1000 surface stations (Zhang et al. 2022) across northern Africa and the eastern Atlantic. With a central focus on improving the understanding and prediction of how smaller-scale tropical weather systems affect larger-scale atmospheric circulations

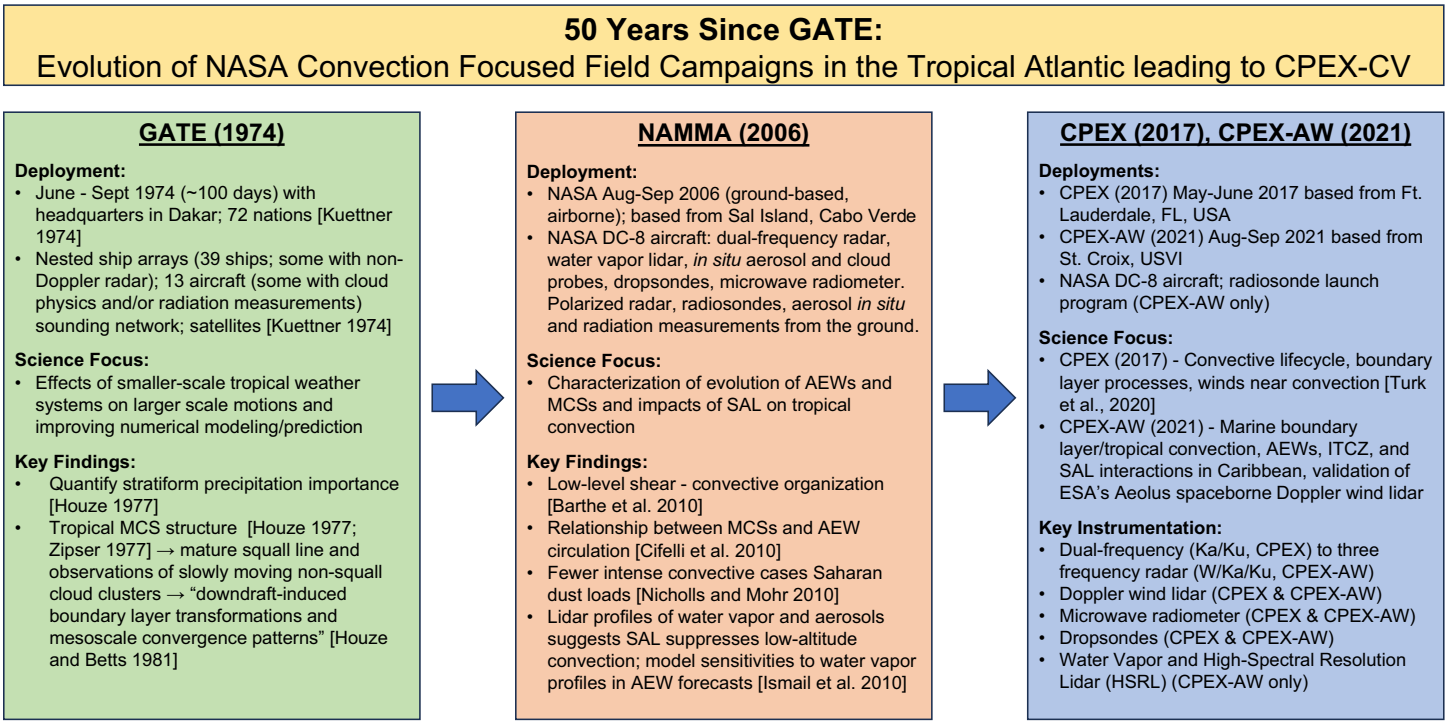

Fig. 1. Brief history and evolution of measurement capabilities and findings from major convection-focused field campaigns in the tropical Atlantic prior to CPEX-CV.

(Kuettner 1974), several seminal papers on organized tropical convective systems established our understanding of stratiform precipitation (Houze 1977), the structure of rapidly moving oceanic squall lines (Houze 1977; Zipser 1977; Leary and Houze 1979), and an appreciation for the distinction of mesoscale up/downdrafts from their smaller-scale counterparts within individual cumulus convective cores, especially as a control on the location of new convective growth (Houze and Betts 1981).

It would be over 30 years before another major NASA field program would visit the eastern Atlantic. In 2006, NASA's contribution to the multiyear, international NASA African Monsoon Multidisciplinary Analysis (NAMMA) experiment (Fig. 1) (Redelsperger et al. 2006) was flying the DC-8 from Sal, Cabo Verde, in August and September instrumented with dropsondes, passive and active remote sensors, and cloud and aerosol in situ probes. NAMMA sampled the large-scale environment, embedded MCSs, and SAL events associated with seven consecutive AEWs transitioning from western Africa to the tropical eastern Atlantic (Zipser et al. 2009). Through these at-the-time unique airborne observations and subsequent modeling experiments, the community gained further understanding of MCS evolution within AEWs (Cifelli et al. 2010), the favorable and unfavorable wave structures for TC genesis (Zawislak and Zipser 2010), and the structure of the SAL (Ismail et al. 2010), including how the SAL limits the development of intense convection (Nicholls and Mohr 2010) and its contended role as a contributor in the prevention of TC genesis (Reale et al. 2009; Braun 2010; Braun et al. 2013).

In many respects, GATE and NAMMA served as key predecessors to the design concept of the CPEX campaign series that enabled convection, AEW, and dust measurements spanning the tropical North Atlantic (Fig. 1). CPEX-AW (2021) built upon the CPEX (2017) campaign based out of Florida with enhanced instrumentation and was originally planned for July 2020 out of Sal Island but was delayed until August 2021 out of Saint Croix, U.S. Virgin Islands, due to the COVID-19 pandemic. The CPEX series established research focal areas on convection, its interaction with aerosols, the SAL, and the marine boundary layer, and how it evolves and feedbacks within large-scale atmospheric waves. Yet, even with a similar instrument payload design to its predecessors, CPEX-CV promised to further advance process-level understanding

in the tropical East Atlantic given the advances in airborne instrument technology, satellite remote sensing capabilities now available to supplement the airborne observations, and the ever-improving numerical models and data assimilation systems capable of ingesting high temporal and spatial resolution satellite and aircraft data. While airborne, satellite, and modeling capabilities for studying tropical convection have advanced significantly since GATE, one constant in all these campaigns was the participation of Dr. Ed Zipser, who celebrated his 40th field campaign while in the field for CPEX-CV (Fig. 2).

FIG. 2. (right) Dr. Ed Zipser honored for his 40th field campaign with (left) CPEX-CV project scientist and former graduate student Dr. Jon Zawislak.

3. CPEX-CV project details

a. Mission objectives, DC-8 payload, ground measurements, and JATAC collaboration. Based out of Cabo Verde, CPEX-CV was well suited to sample interactions between AEWs, Saharan dust outbreaks, and convective systems of various scales as they emerge from the West African coast. CPEX-CV, built upon the aforementioned field campaigns in the region and the CPEX series, targeted the following science objectives (SOs):

SO1: Improve understanding of the interactions between large-scale environmental forcings (e.g., AEWs, ITCZ, SAL, AEJ, and dust plumes) and the life cycle and properties of convective cloud systems, including tropical precursors, in the tropical East Atlantic region.
SO2: Observe how local kinematic (wind) and thermodynamic conditions, including the vertical structure and variability of the MBL, relate to the initiation and life cycle of convective cloud systems and their processes (e.g., cold pools).
SO3: Investigate how dynamical and convective processes affect size-dependent Saharan dust vertical structure, long-range Saharan dust transport, and boundary layer exchange processes.
SO4: Assess the effect of CPEX-CV observations of atmospheric winds, thermodynamics, clouds, and aerosols on the prediction of tropical Atlantic weather systems and validate and interpret spaceborne remote sensors that provide similar measurements.

To meet these objectives, the DC-8 was equipped with a state-of-the-art suite of active and passive remote sensing and in situ instrumentation that enabled synergistic vertical profiling

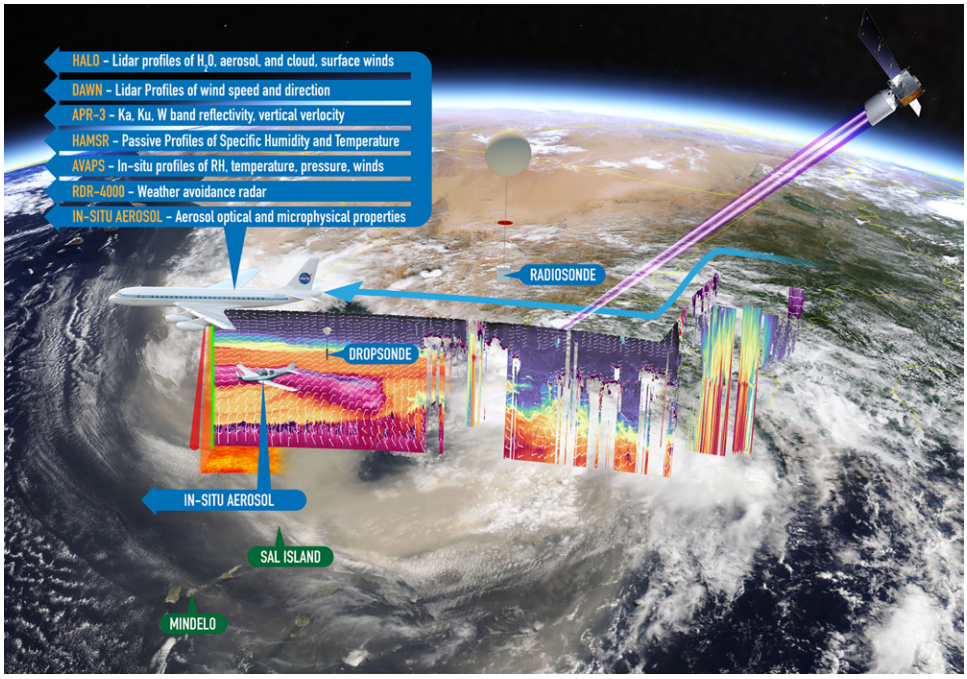

Fig. 3. Conceptual schematic of CPEX-CV operations and payload based out of Sal Island, Cabo Verde.

of the convective, thermodynamic, dynamical, and aerosol environments in the region (Fig. 3). Active sensors included the High-Altitude Lidar Observatory (HALO) lidar (Nehrir et al. 2017; Carroll et al. 2022) that provided aerosol and cloud profiles of backscatter, extinction, lidar ratio, and depolarization using 532-nm high-spectral resolution lidar (HSRL) and 1064-nm elastic backscatter channels, as well as water vapor profiles using the differential absorption lidar (DIAL) technique. The payload also included the Doppler aerosol wind lidar (DAWN) (Bedka et al. 2021; Greco et al. 2020a,b; Kavaya et al. 2014) for 2-μm measurements of horizontal wind speed and direction profiles along the DC-8 flight track. The Airborne Third Generation Precipitation Radar (APR-3) (Sadowy et al. 2003; Durden et al. 2012) provided radar reflectivity and Doppler profile measurements of nonprecipitating anvil and precipitating convective systems at W, Ka, and Ku bands. The High-Altitude Monolithic Microwave Integrated Circuit (MMIC) Sounding Radiometer (HAMSR) provided passive observations of temperature and water vapor with moderate swath under both clear and cloudy conditions (Brown et al. 2011). For in situ measurements, the payload included the Airborne Vertical Atmospheric Profiling System (AVAPS) (Hock and Franklin 1999) dropsonde capability for vertical profiles of thermodynamics and winds and the Cloud, Aerosol, Precipitation Spectrometer (CAPS) (Baumgardner et al. 2001; Spanu et al. 2020) providing aerosol and cloud particle size distributions and particle imaging from 0.5 to 1500 μm. The payload was additionally augmented with the RDR-4000 X-band radar (Harrah et al. 2019) for critical situational awareness and hazard avoidance in and around deep convection. On the ground, radiosonde (Graw DFM-09 model) launches were conducted by the University of Utah from Sal Island three times per day to characterize the diurnal evolution of thermodynamics and winds. Detailed airborne instrument descriptions with nominal data products and resolutions for each instrument are provided in section S.3 in the online supplemental material.

CPEX-CV operations were further enhanced through collaboration with international partners. Coordinated flights with airborne and ground-based platforms as part of the 2022 JATAC operations (Fehr et al. 2023) allowed for the validation of ESA's Aeolus spaceborne wind lidar (Reitebuch 2012) (Fig. 3). These coordinated efforts included DC-8 overpasses of the ASKOS ground validation supersite in Mindelo, Cabo Verde, coordinated by the National Observatory of Athens together with European partners, where an aerosol and cloud

remote sensing facility of Aerosol, Clouds and Trace Gases Research Infrastructure (ACTRIS) operated, continuously collecting lidar profiles of aerosols, clouds, particle orientation, and winds, W-band radar profiles of clouds and precipitation, surface radiation measurements, and radiosonde launches (Marinou et al. 2023). The 2022 JATAC operations also included the Calibration and Validation for Aeolus-Aerosols/Winds (CAVA-AW) campaign that featured a WT10 light aircraft equipped with aerosol size and optical property instrumentation from the University of Nova Gorica (Yus-Díez et al. 2023; Močnik et al. 2023).

b. Mission and modeling support. Modeling, visualization, and remote sensing tools provided CPEX-CV with forecasting and flight planning support and near-real-time situational awareness. Three regional modeling groups supported the campaign with near-real-time forecasts: the University of California, Davis (UC Davis), the University of Utah (UU), and the University of Washington (UW). Each of these groups' models was built upon the mesoscale community's Weather Research and Forecasting (WRF) Model (Skamarock et al. 2019), having identical domains and resolutions (4 km nested in a 12-km grid), but each possessing distinct configurations with different strengths for this region. The UW Unified Wave Interface-Coupled Model (Chen and Curcic 2016), initialized by the European Centre for Medium-Range Weather Forecasts (ECMWF) global analysis, is a fully coupled atmosphere–wave–ocean model that combines WRF with the University of Miami Wave Model (Donelan et al. 2012) and the Hybrid Coordinates Ocean Model (Bleck 2002). Conversely, both the UU and UC Davis models drew from the National Centers for Environmental Prediction (NCEP) Global Forecast System (GFS) global analysis, with UC Davis coupling the WRF Model with a dust module that includes dust–radiation–cloud interactions (Chen et al. 2010, 2015; Huang et al. 2019). Additionally, the U.S. Naval Research Laboratory (NRL)'s regional Coupled Ocean–Atmosphere Mesoscale Prediction System (COAMPS) adjoint model (Doyle et al. 2012, 2019) was employed as a diagnostic tool to identify regions with high sensitivity and observational impact. Finally, ensemble-based sensitivity calculations were carried out daily using ECMWF ensemble output (Torn 2010; Wick et al. 2020) to identify geographic locations where observations could influence the subsequent evolution of the African easterly wave or convection.

Several global models supported CPEX-CV. The National Science Foundation National Center for Atmospheric Research (NCAR) Model for Prediction Across Scales-Atmosphere (MPAS-A) (Skamarock et al. 2012) was run at a cloud-permitting scale (3 km) over the eastern Atlantic region and provided extended (5-day) real-time forecasts. The GFS (Whitaker et al. 2008; Toth and Kalnay 1997) and ECMWF (Persson and Grazzini 2007; Molteni et al. 1996) models were used for longer-term large-scale synoptic forecasts for multiday flight planning. Global aerosol forecasting support was provided by the NASA Global Modeling and Assimilation Office (GMAO) Goddard Earth Observing System (GEOS) (Colarco et al. 2014; Randles et al. 2013; Colarco et al. 2010) and the NRL Navy Aerosol Analysis and Prediction System (NAAPS) (Rubin et al. 2023; Xian et al. 2009).

Data from models were synthesized and presented by a team of student and early career forecasters daily for near- and longer-term planning. Also critical to CPEX-CV was the NASA Jet Propulsion Laboratory (JPL) data portal (Hristova-Veleva et al. 2020, and see section S.4), which allowed for overlaying forecast model output with operational data for developing flight plans, and, by incorporating quicklook images from the DC-8 instrumentation, has continued to serve as a valuable tool in the postfield data analysis phase of the project. Real-time situational awareness was enhanced by expedited high temporal resolution geostationary imagery provided by the University of Wisconsin (http://geoworldview.ssec.wisc.edu) and by two object-based tracking algorithms developed by CPEX-CV early career scientists applied to real-time forecast data: AEW tracker ran on GFS (Lawton et al. 2022) and the Tracking Algorithm for Mesoscale Convective Systems (TAMS) ran on MPAS (Núñez Ocasio et al. 2020a).

c. Field campaign highlights. In CPEX-CV, the DC-8 performed 13 science flights totaling over 90 h in September 2022 (Fig. 4) with over 400 dropsondes released and over 90 radiosondes released from Sal Island. The DC-8 targeted convection and convectively generated cold pools across various scales and environments, including numerous AEWs, several SAL outbreaks, and the ITCZ. Targeting multiple phenomena and science objectives within a single research flight (RF) was common (Table 1). Highlights include sampling convection associated with pregenesis phases of Hurricanes Fiona (RF03) and Ian (RF06 and RF07) and Tropical Storm (TS) Hermine (RF09 and RF10), offshore convection at different times of day (RF05 and RF08), and several Saharan dust events, including an event with a seasonally unprecedented high aerosol optical depth (AOD) > 3.0 at 550 nm (RF09). Additionally, the DC-8 performed four underpasses of the Aeolus satellite, four overpasses of the ASKOS ground site at Mindelo, and two coordinated efforts with the CAVA-AW WT10 including RF07 that provided four levels of measurements: ground-based ASKOS, UNG WT10, NASA DC-8, and Aeolus. With diurnal convective processes and Aeolus underpasses being components of the CPEX-CV science objectives, science operations were divided into two halves based on takeoff time. During the first half of the campaign (RF01-RF07), CPEX-CV targeted the late-morning/afternoon component of the convective life cycle and evening underpasses of Aeolus, while the second half (RF08-RF13) targeted both the overnight dissipation phase of convection and early morning development, particularly adjacent to the West African coast. In the following sections, the unique integrated measurements provided by the CPEX-CV payload are highlighted in the context of our science objectives for select flights, including convection associated with a potentially developing AEW (RF02), a SAL outbreak (RF03), and offshore convection near dust gradients (RF09). Section S.2 provides an overview of how primary features targeted during September 2022 compared to climatology.

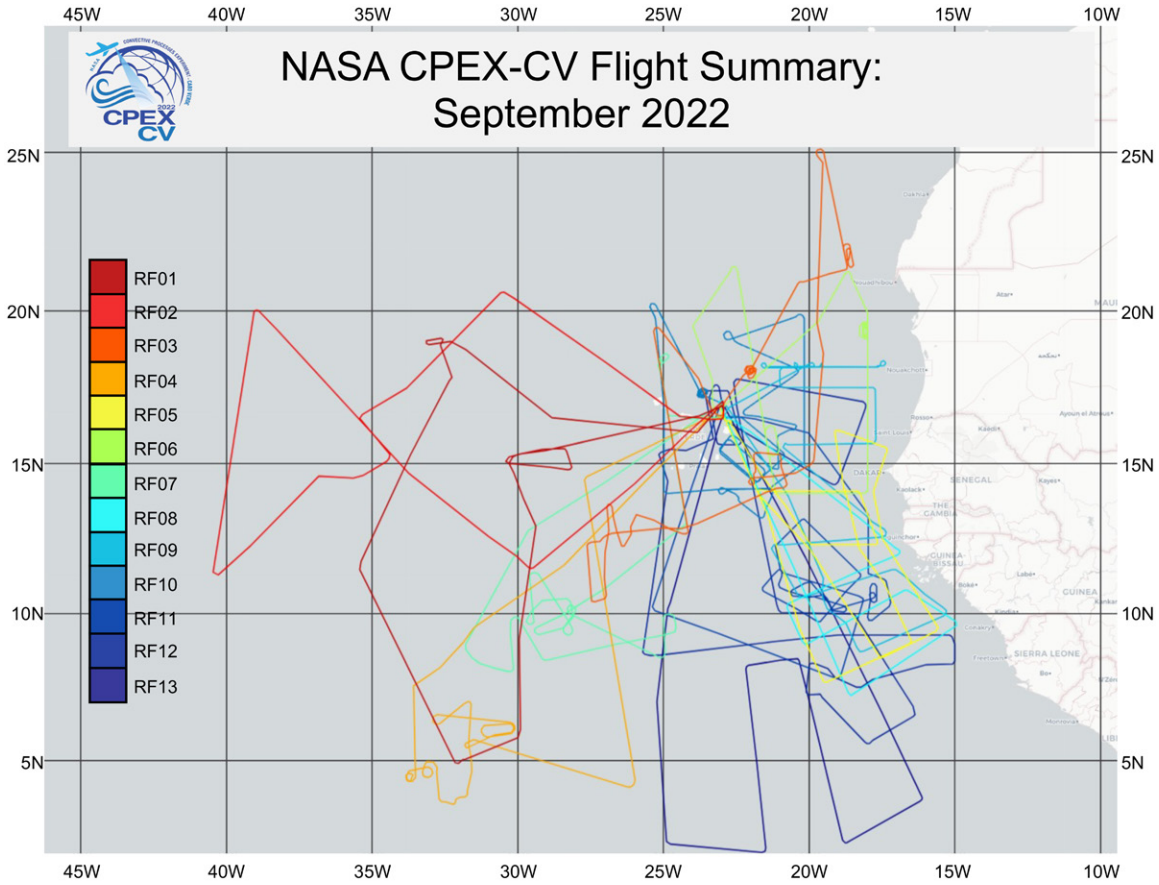

Fig. 4. Overview of DC-8 flight tracks from CPEX-CV during September 2022.

Table 1. Primary science and validation targets for the 13 CPEX-CV RFs.

Research flight	Science target/validation
RF01—6 Sep 2022	AEW with mature MCS, SAL with dust, *Suomi NPP*
RF02—7 Sep 2022	AEW with mature MCS, ASKOS overpass
RF03—9 Sep 2022	AEW with scattered convection, SAL with dust, dust in MBL, ASKOS overpass, Aeolus/*CALIPSO*/*Suomi NPP* underpasses
RF04—10 Sep 2022	ITCZ, scattered convection, Aeolus underpass
RF05—14 Sep 2022	Offshore convection, mature MCS
RF06—15 Sep 2022	Dust outbreak, *Landsat-9* and Aeolus underpass, coordination with CAVA-AW WT10
RF07—16 Sep 2022	AEW with scattered convection, Aeolus underpass, coordination with CAVA-AW WT10, overpass of ASKOS
RF08—20 Sep 2022	Scattered offshore convection
RF09—22 Sep 2022	AEW with mature MCS, offshore convection with mature MCS, massive dust outbreak, dust in MBL
RF10—23 Sep 2022	AEW with mature MCS, dust outbreak, ASKOS overflight
RF11—26 Sep 2022	AEW with mature MCS
RF12—29 Sep 2022	Underpass of *NOAA-20* ATMS, CrIS, and VIIRS, TROPICS Pathfinder, *MetOp-B* IASI; *MetOp-B* ASCAT; ISS TEMPEST-D/COWVR
RF13—30 Sep 2022	ITCZ with scattered convection, AEW with mature MCS

d. RF02—AEW–convection–dry air. The first two flights of CPEX-CV featured two consecutive days of sampling the same AEW, with RF02 (7 September 2022) occurring after the National Hurricane Center (NHC) declared it Invest 95 L with a medium 60% probability of tropical cyclogenesis in the next 2–5 days. This scenario provided an opportunity to target SO1 and SO4 by collecting the unique measurements that CPEX-CV was designed to obtain coincident measurements of convective structure with its near-storm environment. At the start of the flight, a large convective band was observed north of the potentially developing circulation center (Fig. 5), along with a possible intrusion of SAL dry air from the south-southwest. Dry air can suppress convection (e.g., Wang and Sobel 2012) through entrainment (e.g., Ridout 2002) and enhance evaporatively driven downdrafts (e.g., Emanuel 1989) or in an overall reduction in convective available potential energy (CAPE), thus reducing convective activity within the wave's circulation center. The potential detrimental effects of this dry environment on TC genesis were on display on this flight, where the dry air limited convection near the center of the wave's cyclonic circulation. The flight plan covered the wave-relative environment, including passes through the band of dry air and sampling areas of the convective regions to the north and south of the circulation center.

The driest midlevel air was sampled with the 1543 UTC dropsonde (Fig. 5c) and dry air appeared to intrude into the wave's circulation center at 1616 UTC (Figs. 5a,d), albeit relatively moister than to the south. As the DC-8 flew northeastward toward the circulation center between ~1545 and 1615 UTC (Fig. 5a), the remote sensing instrumentation sampled the intense convective line from 1555 to 1605 UTC in the vicinity of the dry air (Fig. 6). During this period, mature stratiform precipitation with an intense bright band seen in Ku-band radar reflectivity (Fig. 6c) transitioned into intense and mature but relatively shallow convection (Figs. 6c,d) as the plane encountered the dry (Fig. 6b) and moderately dusty (Fig. 6a) midlevel (2–3 km) air sampled between 1542 and 1552 UTC approaching the circulation center (Fig. 5a). Adjacent DAWN winds (Fig. 6c) highlight the westerly flow corresponding to the dry midlevel air observed in both HAMSR and dropsonde data (Fig. 6b) while revealing the presence of vertical wind shear to the south of this precipitating band (Fig. 6c) in an area with limited dropsonde coverage (Figs. 5a and 6).

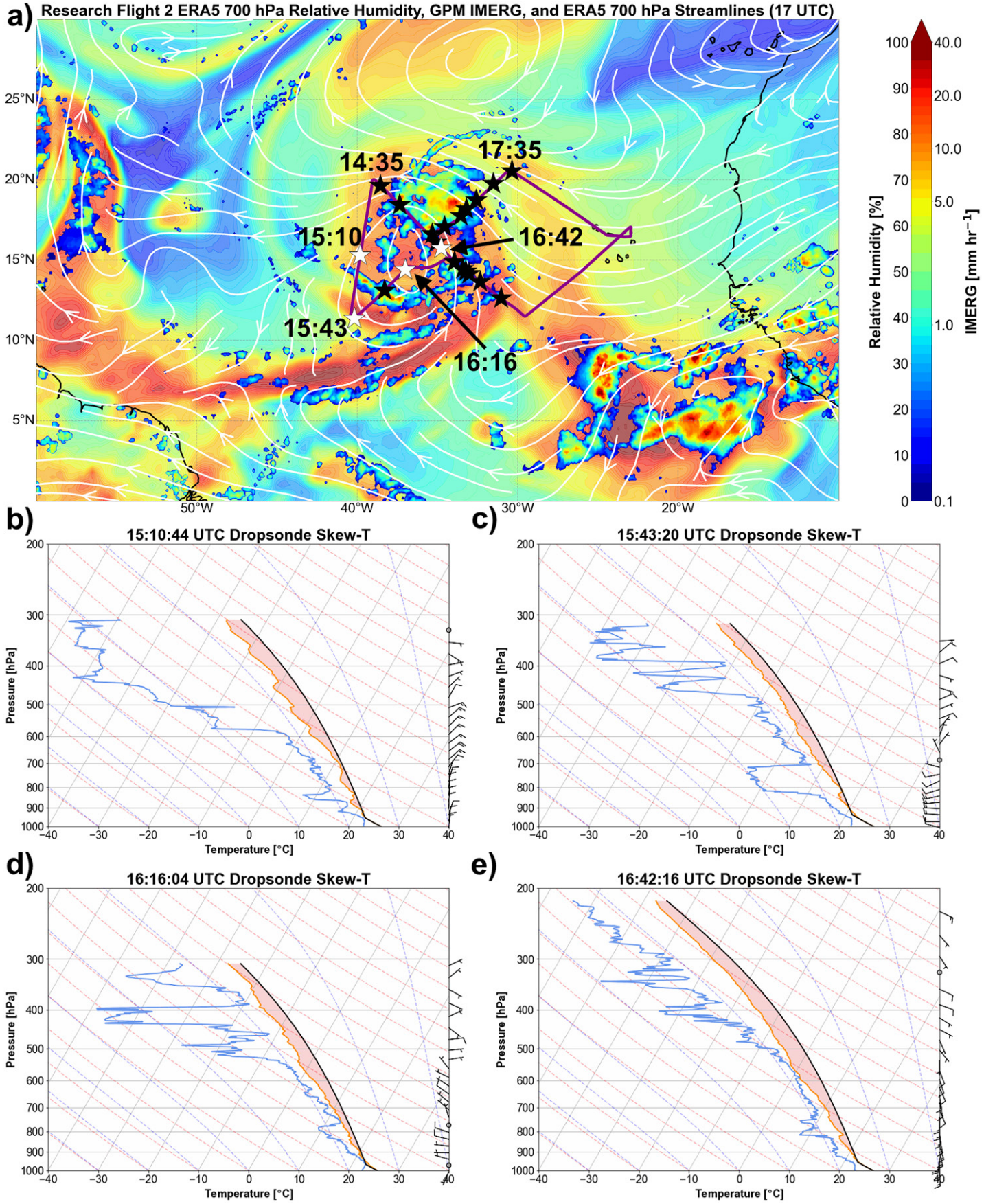

FIG. 5. (a) Overview of RF02 flight track (purple line) with IMERG rain rates (mm h^{-1}; color shading) at 17 UTC, ERA5 700-hPa streamlines (white lines) and relative humidity (%; transparent color shading) valid at 17 UTC, and dropsonde locations (stars) with (b)–(e) dropsonde skew *T* values shown at select times in UTC (white stars) along the flight track, where the blue line is dewpoint temperature, the red line is temperature, and the black line is the temperature of undiluted air parcels lifted from the surface. The area in red shading represents CAPE.

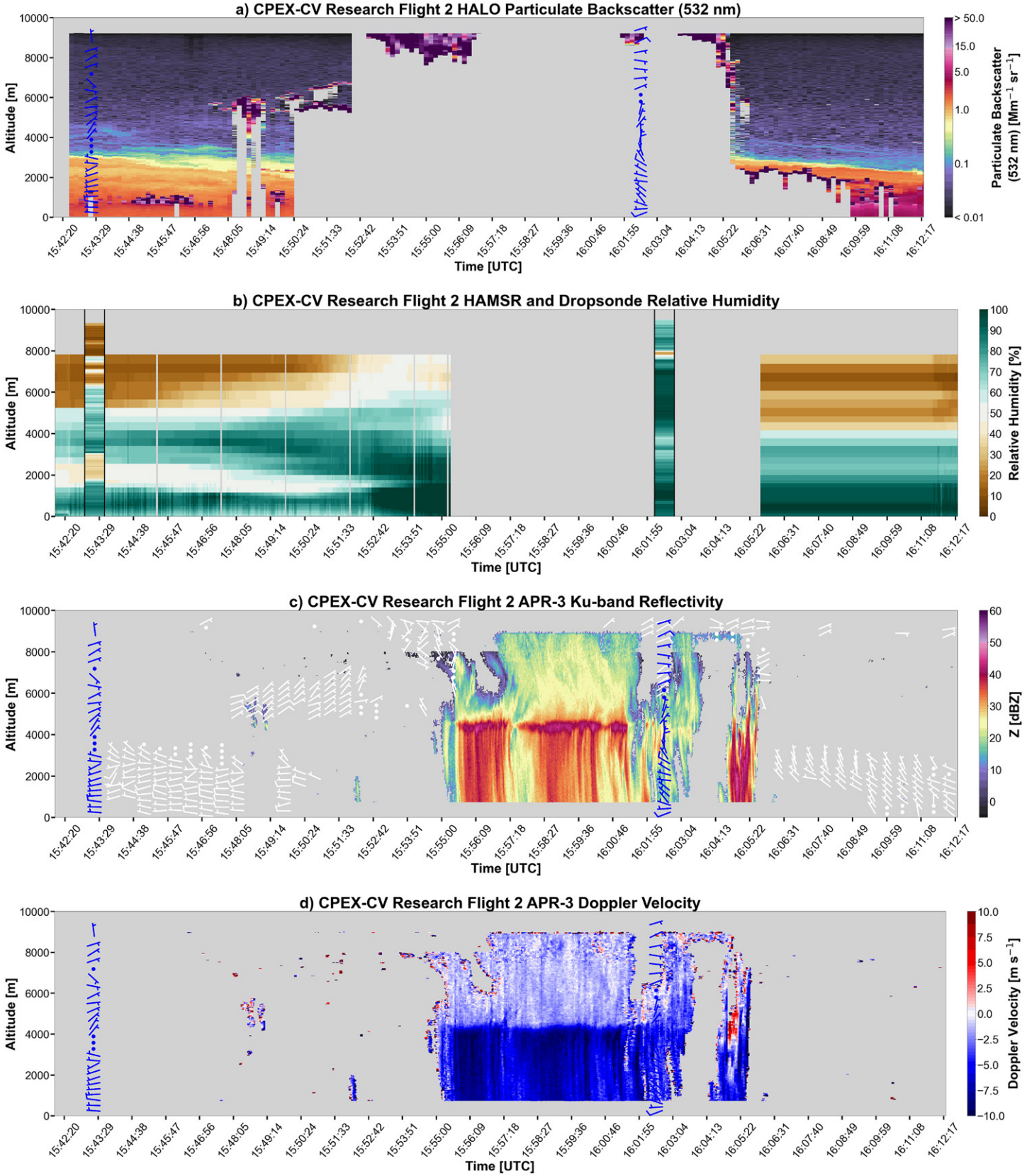

FIG. 6. Curtain plot individually showing (a) HALO particulate backscatter at 532 nm, (b) HAMSR and dropsonde relative humidity, (c) APR-3 Ku-band radar reflectivity with DAWN winds (white barbs), and (d) APR-3 Ku-band Doppler velocity during the 1542–1611 UTC flight leg of RF02 (see Fig. 5a). Overlaid on (a), (c), and (d) are dropsonde winds (blue barbs).

After passing through the center of the wave circulation (Fig. 5a), APR-3's W band (Fig. 7b), starting around 1650 UTC, sampled thick anvil limiting HALO and DAWN retrievals near the precipitating system (Fig. 7a); although above (>8 km), a potential influence

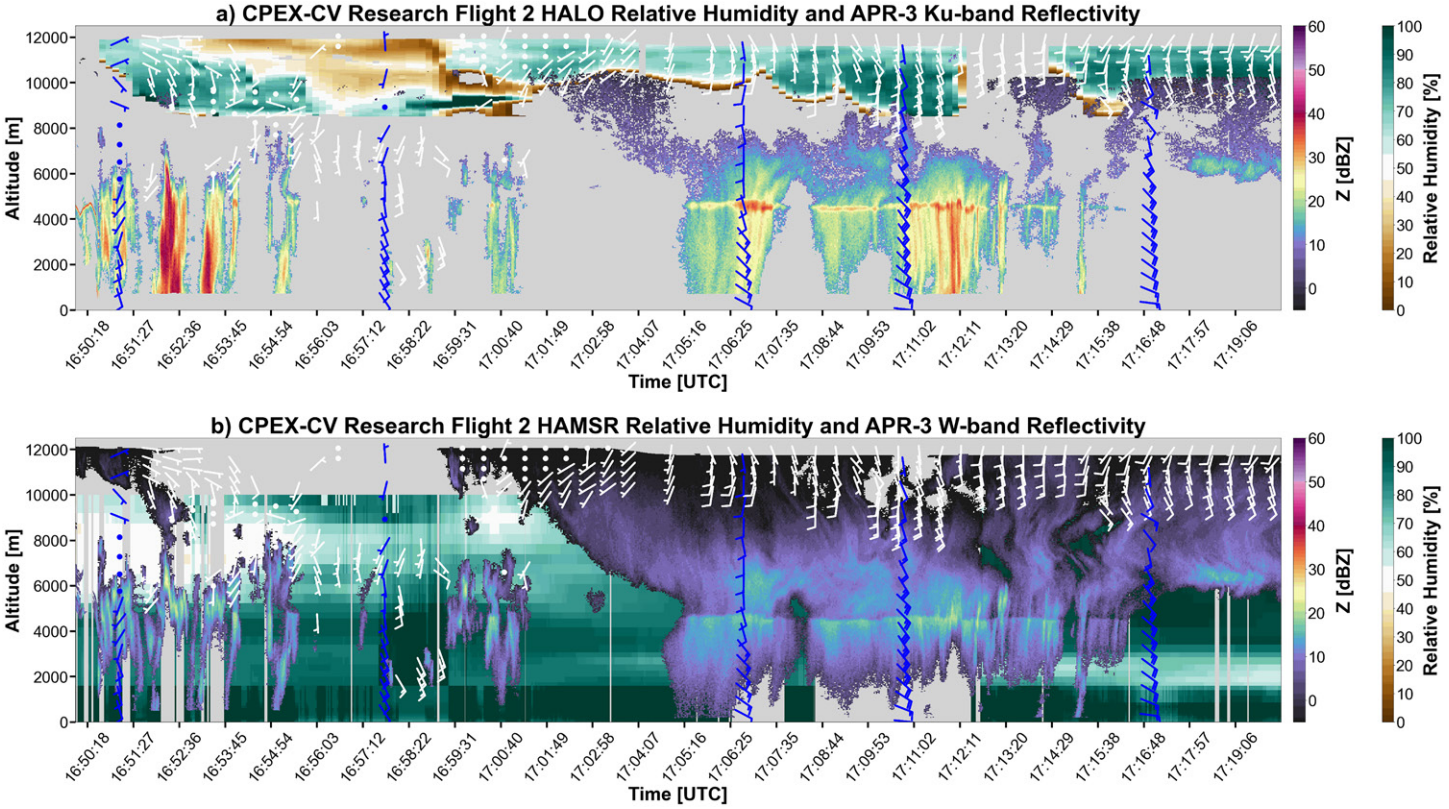

Fig. 7. Curtain plot as in Fig. 6, but overlaid datasets showing (a) HALO relative humidity with APR-3 Ku-band radar reflectivity and (b) HAMSR relative humidity with APR-3 W-band radar reflectivity during the 1650–1719 UTC flight leg of RF02 (see Fig. 5a). Overlaid are DAWN (white barbs) and dropsonde (blue barbs) winds.

of moistening aloft by the convection is observed (Fig. 7b). While the DC-8 passed to the east of the deepest convection according to satellite imagery (1650–1730 UTC flight leg, Fig. 5a), APR-3 continued to sample a variety of convective life cycle stages, with Fig. 7 showing relatively shallow convection as the DC-8 crossed over the midlevel dry area closer to the wave's circulation center (Fig. 5a) and then toward decaying convection with a discontinuous bright band at Ku band (Fig. 7a). Frequent releases of dropsondes (blue barbs, Fig. 7) across this flight leg in areas with limited DAWN coverage highlight the sheared environment in which this convection was in addition to the presence of dry midlevel air in its vicinity (Fig. 7b).

The hypothesis for this flight is that the sampled dry slot is influential to the likelihood of further development and ultimate TC genesis. Aggregated model and satellite data (Fig. 8) provide more evidence of the fate of the wave and associated convection after RF02. Weakening convection (from IMERG) in the vicinity of the dry air (model relative humidity) is observed from 0000 to 1800 UTC 8 September 2022. At the same time, this pattern evolved such that most of the remaining convection was concentrated to the north of the circulation center. This Invest ultimately did not lead to TC genesis, but the rare observations collected during CPEX-CV will enable detailed investigation into the role of the dry air intrusion in the convective evolution associated with a strong nondeveloping AEW trough.

e. RF03—Saharan dust outbreak. Of the thirteen CPEX-CV research flights, three (RF03, RF06, and RF09) sampled Saharan dust events as a primary focus. The third flight of CPEX-CV shifted focus to sampling vertical variability within the Saharan dust plume and interaction with convection. Observations acquired during RF03 provide an opportunity to understand the evolution of dust particle size distributions of varying dust loading within and above the

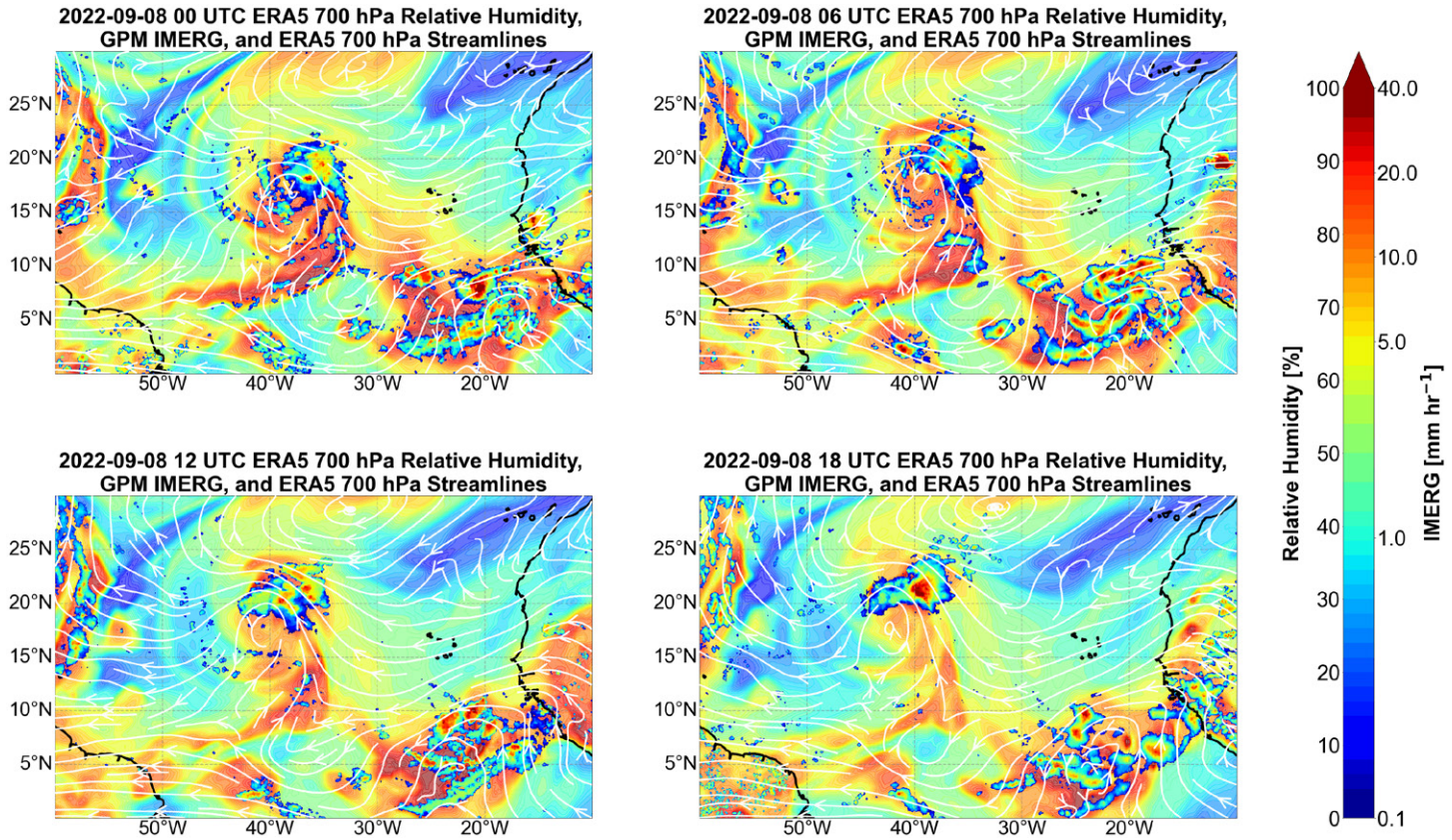

FIG. 8. IMERG rain rates (mm h^{-1}; color shading) and *GEOS-5* 700-hPa streamlines (white) and relative humidity (%; transparent color shading) every 6 h starting 0000 UTC 8 Sep 2022 immediately following the conclusion of RF02.

MBL with transport, impact of moisture on dust optical properties, and interaction with a line of convection that would become Hurricane Fiona, relevant to all CPEX-CV science objectives.

Previous in situ observations of African dust have shown supercoarse-sized (diameter > 10 μm) dust particles defy classical Stokes' settling theory (Maring et al. 2003; Colarco et al. 2003; Reid et al. 2003) and are transported over 4000 km to the Caribbean (Middleton et al. 2001; Weinzierl et al. 2017; Denjean et al. 2016; van der Does et al. 2018) and beyond to the Americas (Swap et al. 1992; Liu et al. 2008). Uncertainty remains in the current understanding of dust transport phenomena, the relationship of dust vertical profiles to meteorological processes, and the sensitivities of coupled processes to dust mineralogy, particle size distribution, or optical properties.

On 9 September (RF03), the NASA DC-8 targeted a moderate Saharan dust outbreak and its borders (Fig. 9). The flight track cut directly across the axis of the dust plume along the 20°W longitude line (Figs. 9a,d; maximum optical depth ~0.6 at 532 nm observed by HALO), from subsidence-induced dry air to the north to the edges of tropical convection to the south (Fig. 9b). Included were two vertical profiles to profile the dust with CAPS, sampling along convergence lines and ending with underlights of the Aeolus wind lidar beam path (Fig. 9a). Active remote sensing on the NASA DC-8 was crucial to understanding the nature of this event, including HALO water vapor mixing ratio and DAWN wind vectors (Fig. 9c) as well as HALO's aerosol backscatter (Fig. 9d). Notable in this transect are dust layers between 20° and 23°N that also contain appreciably enhanced water vapor. Studies on dust-radiation effects have suggested that dust effects on the infrared radiative budget are dwarfed by cotransport with water vapor (Wong et al. 2009; Gutleben et al. 2019), emphasizing the need for coincident observations of dust and the moisture field in evaluating these effects. While dust is prevalent throughout this SAL, dust backscatter of varying intensity is located

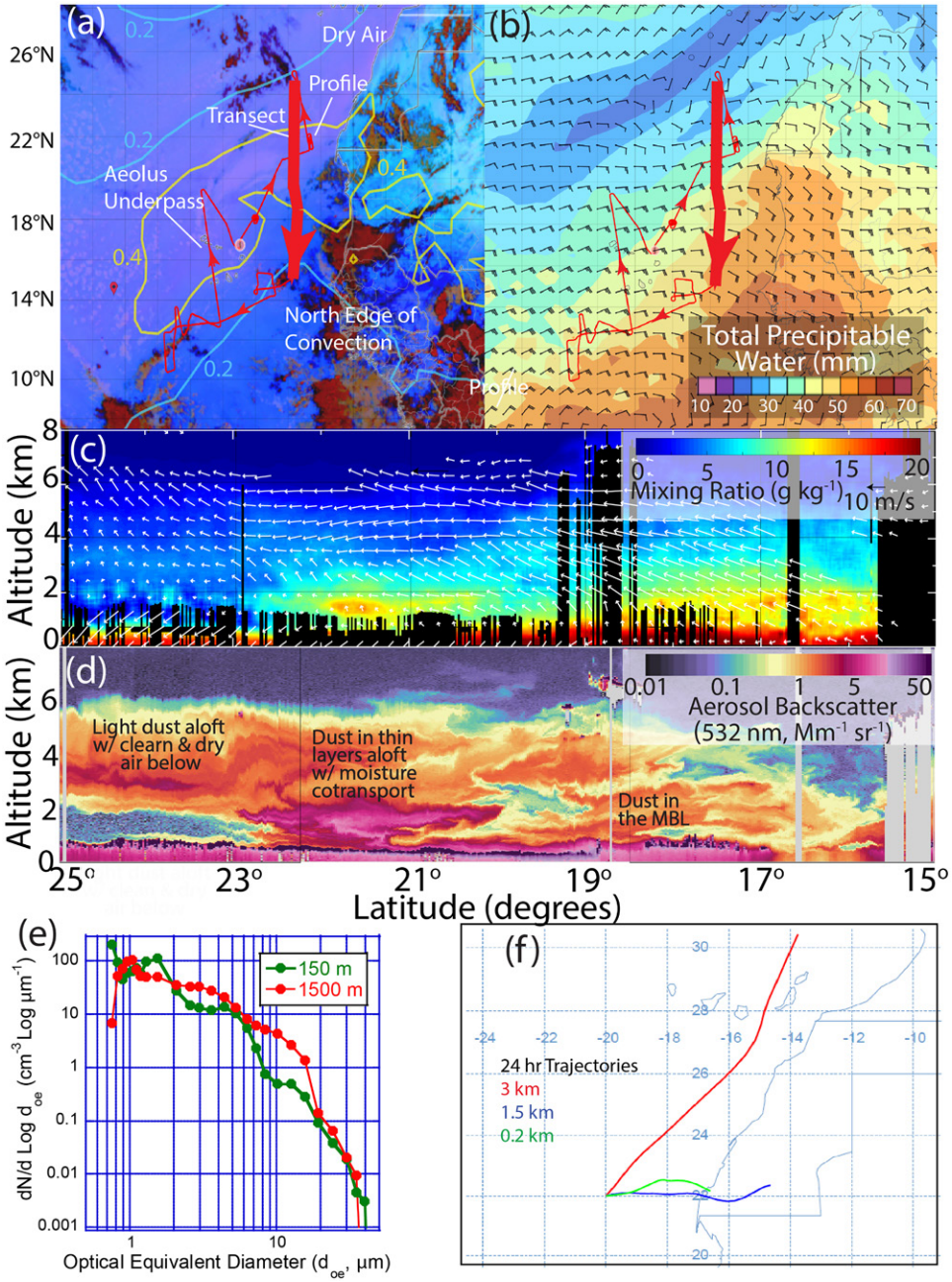

Fig. 9. (a) DC-8 track (red) and AOD from the International Cooperative for Aerosol Prediction (ICAP) consensus over Meteosat second generation (MSG) Spinning Enhanced Visible and Infrared Imager red–green–blue (SEVIRI RGB), (b) Navy Global Environmental Model (NAVGEM) total precipitable water (TPW) and 850-mb winds, (c) HALO water vapor and DAWN wind vectors, (d) HALO aerosol backscatter, (e) CAPS particle size distributions obtained between 1415 and 1430 UTC, and (f) GFS backtrajectories from an in situ maneuver from RF03 on 9 Sep 2022. Subcomponents of the flight shown in (c) and (d) are indicated by the thick red line in (a) and (b).

within several thin layers of only several hundred meters. Along gradients in both dust and moisture observed by HALO, DAWN measured regions of horizontal and vertical wind shear within these complex features. These observations are inconsistent with the standard (Karyampudi et al. 1999) conceptual model that dust layers originating from the Sahara emerge from the coast in well-mixed and dry environmental conditions.

Aerosol backscatter is the most enhanced in the MBL (<500 m altitude) between 19° and 21°N and further to the south between 17° and 19°N, and dust is inferred to be mixed into the MBL from the HALO aerosol-type product. Low depolarization ratios observed by HALO suggest this event is dominated by "spherical particles" and suggest the presence of

hygroscopic dust within and above the MBL. This finding indicates the likelihood of evolution of dust optical properties during transport due to the uptake of water by dust particles. A component of Saharan dust is from source regions that are dry lake beds (Westphal et al. 1987; Prospero et al. 2002) and maybe coated by crustal salts (Twohy et al. 2009), which would make those dust particles more hygroscopic. Notable differences in dust size are also found between the MBL and elevated layers (Fig. 9e). Smaller particles in the MBL may be due to scavenging but equally may be part of an observation artifact; if particles are covered in water, then their optical properties may change, which in turn changes the response function of the wing-mounted optical particle counters used to measure them.

Backward trajectories (Fig. 9f) from the in situ profile indicated in Fig. 9a help explain the intricate dust and water vapor patterns, with air in the MBL originating from a different region than at higher altitudes, underscoring the uniqueness of each dust outbreak, as the vertical structure, loading, and composition can be an amalgam of multiple source regions. Finally, as part of RF03, the DC-8 performed a vertical profile to sample a developing line of convection located at 12°N, 25°W. Sampling this event was compelling because it interacted with dust-laden SAL air to the northwest with clean air to the southeast. This convective line eventually would develop into Hurricane Fiona (Fig. 10) and, thus, an interesting case study for investigating the coupling between aerosol–cloud–convection in the tropical East Atlantic that was targeted during CPEX-CV.

f. RF09—Offshore convection, dust–TC interactions, and data assimilation. RF09 was the first of two consecutive flights (RF09 and RF10) targeting convection that developed into TS Hermine in the offshore region near the western African coastline. Data collected from RF09 were relevant to all CPEX-CV science objectives and provided opportunities to study the unique case of interactions among offshore convection, AEW, and a major Saharan dust outbreak that influenced the formation of TS Hermine.

g. Offshore convection. The climatological rainfall is higher offshore of the West African coast than inland, affected by the offshore propagations of MCSs and AEWs (Laing and Fritsch 1993; Zipser 1994; Hamilton et al. 2017; Núñez Ocasio et al. 2020a; Wu et al. 2024). Despite this high offshore maximum being a common feature here and in other tropical monsoonal regions (e.g., Biasutti et al. 2012; Houze et al. 2015; Ogino et al. 2016), the underlying mechanisms that enhance offshore rainfall remain unclear (Hamilton et al. 2017; Fang and Du 2022). The challenges in understanding offshore rainfall partly arise from a lack of observations of three-dimensional atmospheric structure around the coastline. CPEX-CV provided unique observations to investigate these mechanisms by capturing offshore rainfall near the West African coastline and its associated environment during different synoptic conditions and different times of the day.

RF09 on 22 September successfully measured the interactions among an AEW coupled to an MCS, the West African monsoon (WAM), land breeze, offshore rainfall, and a Saharan dust outbreak. Simultaneous tracking of the MCS (via TAMS; Núñez Ocasio et al. 2020a) and the AEW (Lawton et al. 2022) showed deep convection initially coupled to the AEW, with the MCS propagating faster than the speed of the wave up to the point it started reaching the coastline the morning of 22 September (Fig. 11). The cyclonic circulation of this strong AEW was centered onshore near the coastline around 14°N and 16°W in the morning (Fig. 11b), with the MCS partially detached from the center of the wave trough (Figs. 11b,c), suggesting an influence of coastal mechanisms (i.e., WAM, coastal convergence, and land breeze) on maintaining the systems. As the AEW slowly moved westward throughout the day (Fig. 11a), the monsoonal onshore flow around 10°N and 16°W was strengthened compared to 0700 UTC (Fig. 11b), and the wave circulation transported

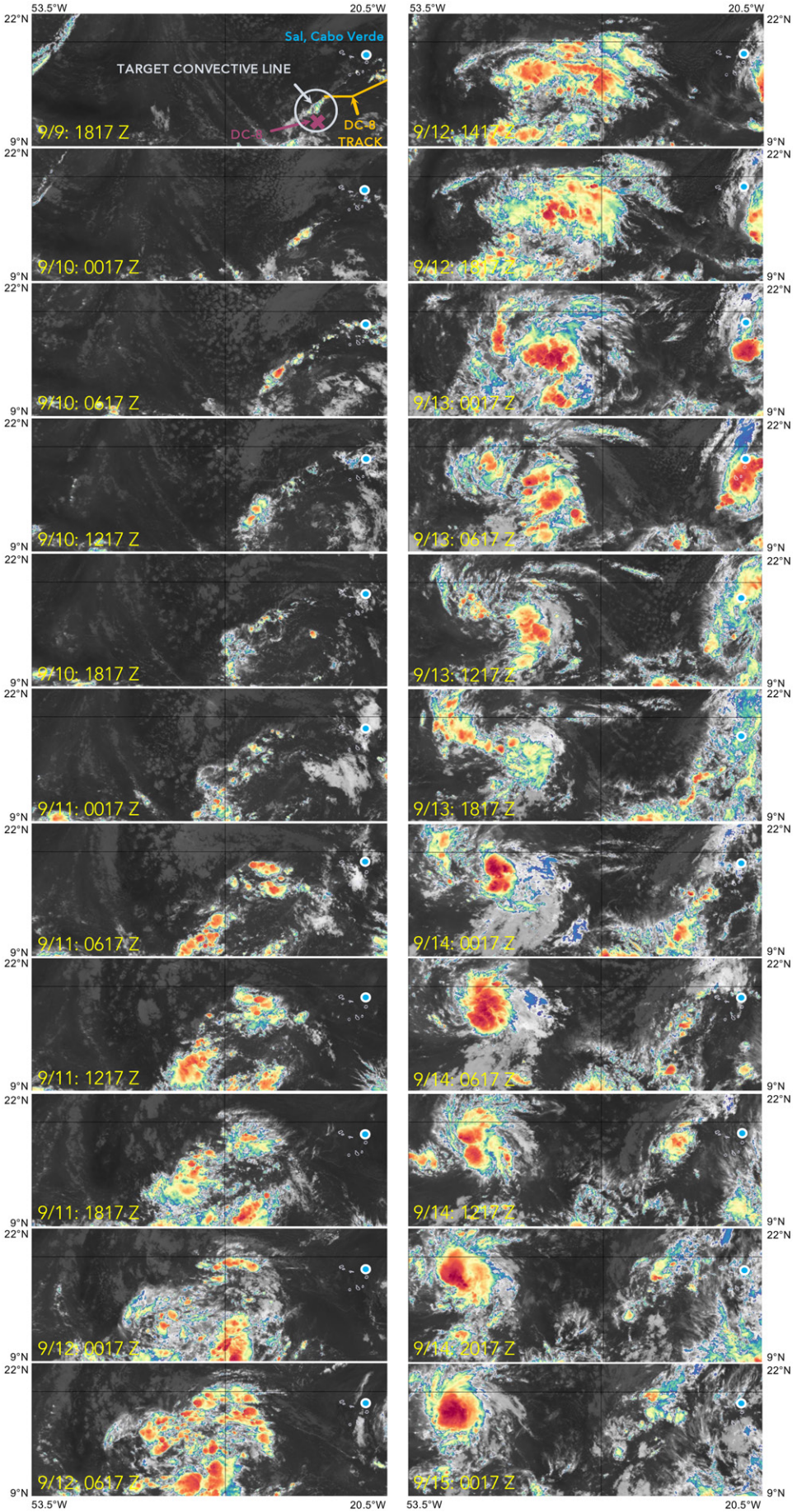

Fig. 10. MSG *Meteosat-11* 11-μm imagery time series of the development of the convective line on RF03 on 9 Sep 2022 into Hurricane Fiona (2022) beginning 14 Sep 2022.

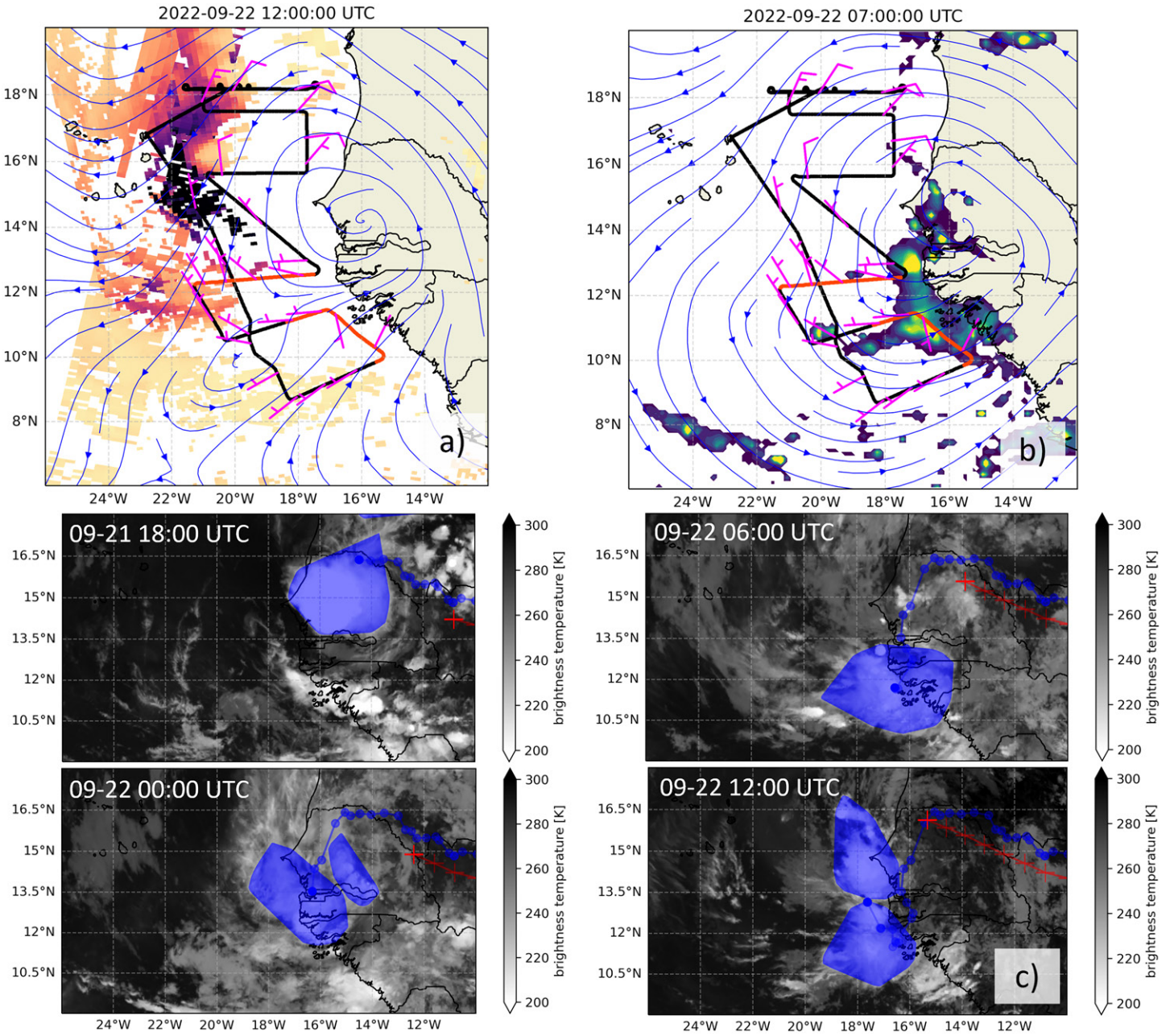

Fig. 11. (a),(b) Track of RF9 (black lines with red in (b) indicating legs highlighted in later figures) and synoptic condition on 22 Sep. (a) 600-hPa ERA5 streamlines at 1200 UTC (blue contours), dropsonde horizontal winds at 600 hPa (magenta wind barbs), and *Terra* and *Aqua* 550-nm AOD at 1130 and 1430 UTC (shaded). (b) ERA5 850-hPa streamlines (blue), dropsonde horizontal winds at 1000 hPa (barbs), and IMERG rainfall at 0700 UTC (shaded). (c) Meteosat brightness temperature (shaded) and the tracks of MCS (blue) and AEW (red) at 1800 UTC 21 Sep and 0000, 0600, and 1200 UTC 22 Sep.

Saharan dust westward and equatorward into the Atlantic Ocean, leading to a major dust outbreak, marked by high AOD (Fig. 11a).

An MCS formed inland near this AEW on 20 September (not shown). Simultaneous tracking of the MCS (via TAMS; Núñez Ocasio et al. 2020a) and the AEW (Lawton et al. 2022) showed the convection initially remained coupled to the AEW, with the MCS propagating faster than the speed of the wave up to the point it started reaching the coastline in the morning of 22 September (Fig. 11c). MCSs that propagate offshore often weaken as they cross the coastline (DeLonge et al. 2010), but those that remain intense and long-lived over the coast, such as in this case, are likely to be associated with an AEW (Núñez Ocasio et al. 2020b). While stalling near the coastline, the MCS partially detached from the center of the wave trough, separating into two convective cloud regions (Fig. 11b) and an overall reduction in area. This detachment

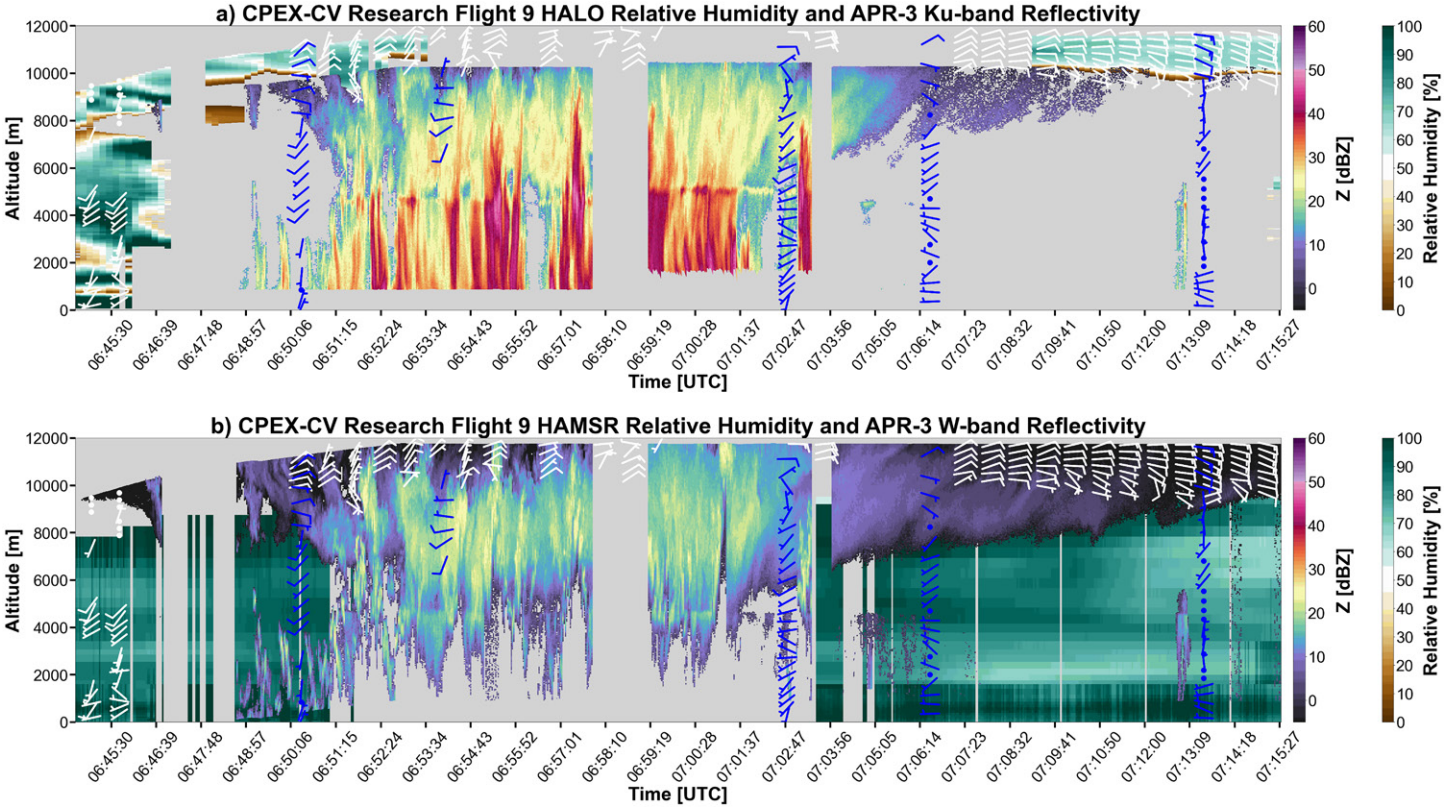

Fig. 12. As in Figs. 6 and 7, showing curtain plots of (a) HALO relative humidity with APR-3 Ku-band radar reflectivity and (b) HAMSR relative humidity with APR-3 W-band radar reflectivity during the 0645–0714 UTC flight leg of RF09 (southern red track in Figs. 11a,b). Overlaid are DAWN (white barbs) and dropsonde (blue barbs) winds.

from the wave suggests coastal mechanisms on maintaining the system and/or interacting with it before it continued expanding and moving northward with the center of the AEW.

The offshore coast–parallel flight leg around 0700 UTC (southern red track in Figs. 11a,b) showed that the MCS contained convective cells at varying life cycle stages within this APR-3 snapshot (Fig. 12). The Ku-band data highlight intense convection with reflectivity greater than 40 dBZ extending above 8-km altitude and decaying cells contributing to a discontinuous radar bright band (Fig. 12a). Encountering this offshore convection from the south at 0645 UTC, DAWN winds show the monsoonal onshore flow up to 1 km with high relative humidity (>90%) as retrieved from HALO. Closer to the convection, as the anvil thickens (Fig. 12b), DAWN winds are limited to the highest few kilometers of the flight leg. Within those upper levels of the anvil (highlighted in the APR-3 W-band data in Fig. 12b), DAWN reports generally westerly flow, but with variability in direction and speed owing to proximity to the deepest convective cores as this system detrains moisture into the upper atmosphere (see HALO relative humidity in Fig. 12a; 0650–0653 UTC). The 0650 UTC dropsonde winds revealed vertical wind shear throughout the column, owing in part to this detraining easterly flow aloft compared to westerly below and the abrupt shift to southerly flow near and within the vicinity of the convective system possibly owing to convective outflow. As the DC-8 turned westward away from the coast and convection at 0704 UTC (southern red track in Figs. 11a,b), the thick extensive anvil, as uniquely highlighted in the APR-3 W-band data (Fig. 12b), limited full vertical profiles of DAWN and HALO data. However, HAMSR shows an increasingly dry layer between 2 and 3 km extending farther from the coast. The influence of this near-storm environment on convective structure is a key focus of CPEX-CV in the context of offshore convection, as seen here as well as within other varying environments throughout the campaign. Far from a classic squall-line scenario, the multifrequency APR-3 data provide a unique view into the mode, intensity, and hydrometeor profiles of convection in this region.

This flight uniquely captured near-surface monsoonal onshore flow meeting an offshore land breeze, a hypothesized mechanism for creating convergence along the coastline, providing mechanical forcing for convection to grow and propagate offshore (Houze et al. 1981; Grossman and Durran 1984; Mapes et al. 2003; Peatman et al. 2023). DAWN data, in particular, reveal the detailed structure of horizontal winds around the coastline, showing monsoonal onshore flow when the DC-8 flew zonally toward the coastline around 12°N between 0745 and 0815 UTC (Fig. 13a). The westerly onshore flow extends from the surface to about 2 km, and its strength and vertical depth increase toward the coastline, perhaps due to the effect of the AEW near the coastline. The presence of offshore convection limits data retrieval for the DAWN near the coastline in the lower troposphere; however, dropsonde data at 1000 hPa near the coastline (Fig. 13b; around 15°W and 10°N) show near-surface onshore winds continue

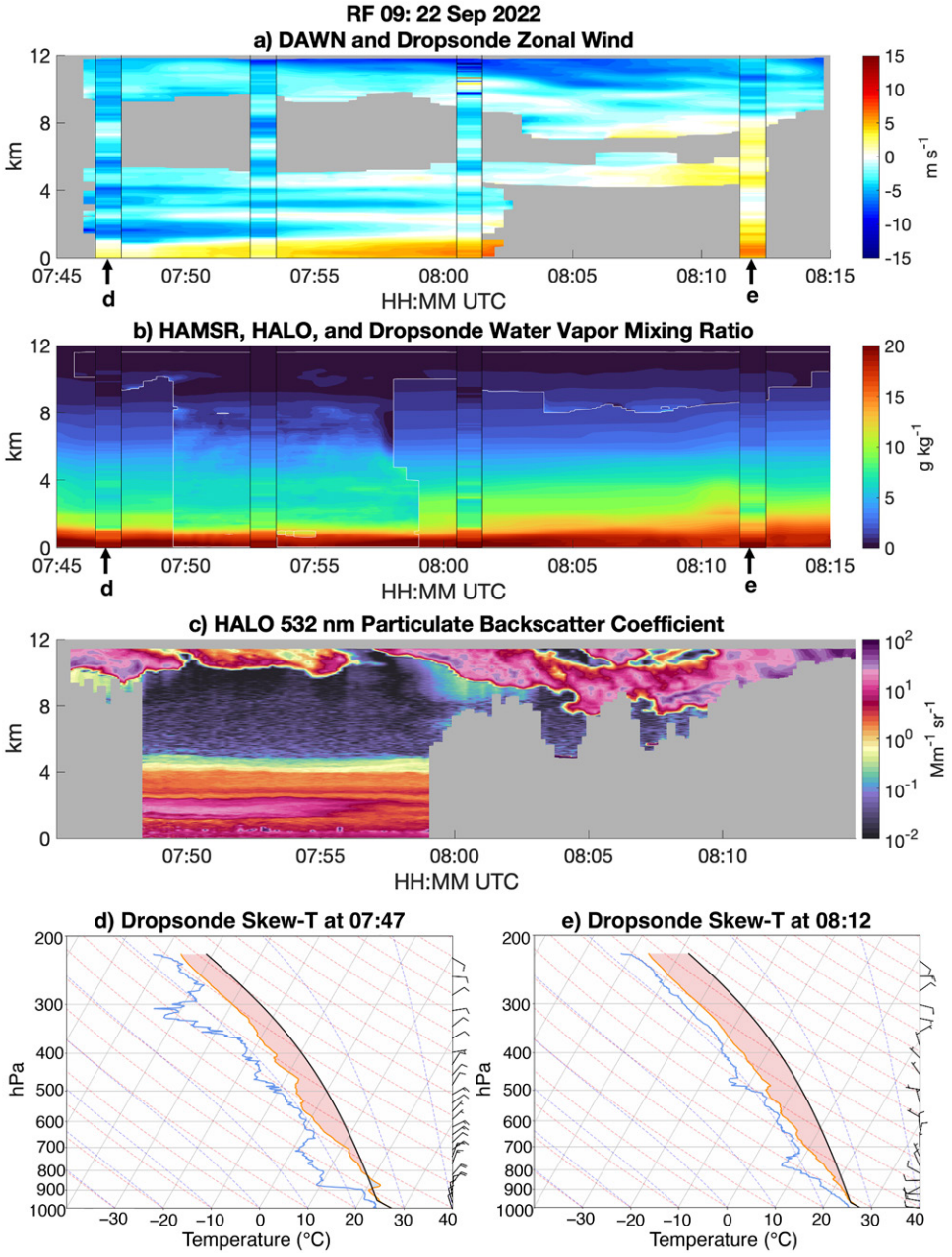

Fig. 13. Synergistic atmospheric profiles from multiple instruments on board DC-8 from 0745 to 0815 UTC 22 Sep 2022 (northern red track in Figs. 11a,b), during RF09. (a) Zonal wind from DAWN and dropsondes (m s^{-1}) where dropsonde values are overlaid on top of DAWN data in vertical columns. (b) HAMSR, HALO, and dropsonde water vapor mixing ratio. HALO data are overlaid on top of HAMSR data in areas enclosed by a white line. (c) HALO 532-nm particulate backscatter coefficient. (d),(e) Skew *T* diagram of dropsonde data at 0747 and 0812 UTC.

to strengthen near the coastline. There is also a sign of a density current from convection and/or land breeze (offshore flow) that is captured by a dropsonde (Figs. 11a,b), which collides with the monsoon onshore flow to strengthen the coastal convergence, suggesting that the monsoon–land breeze mechanism may be playing a role in offshore convection propagation and maintenance.

HALO and HAMSR data also reveal the effects of the Saharan dust layer on thermodynamic profiles. HALO data show that a high concentration of dust appeared offshore between 1 and 5 km around 0748–0759 UTC, while backscatter associated with anvil cirrus was observed above 8 km (Fig. 13c). HAMSR, HALO, and dropsonde data further show that this dust layer is associated with a sharp decrease in water vapor mixing ratio and an inversion layer (Figs. 13b,d). Near the coastline, clouds resulting from convection limit the coverage of data from HALO, but HAMSR provides continuous data that show the deepening of the moist layer that is associated with the offshore MCS and WAM (at around 0810 UTC). The consistent deepening of the mixed layer and higher saturation of midtropospheric air is shown by the dropsonde data near the coastline (i.e., northern red track in Figs. 11a,b), although the depth of the mixed layer appears overestimated by HAMSR (Fig. 13e). The dropsonde data near the coastline also show that the inversion layer no longer exists, eliminating convective inhibition and increasing CAPE. These data together are particularly relevant to SO1 and suggest that the SAL created thermodynamic inhibition to convection development offshore, while the thermodynamic environment near the coastline was more supportive for the growth of convection on 22 September 2022.

h. Dust–TC. Later in RF09, the DC-8 focused on sampling the Saharan dust event that wrapped around the AEW and into the developing tropical convective system beginning around 0800 UTC with potential influences on TC development (Dunion and Velden 2004; Evan et al. 2006; Evan and Mukhopadhyay 2010; Lau and Kim 2007; Reale et al. 2009, 2011; Xian et al. 2020) and tracks (Chen et al. 2015; Nowottnick et al. 2018). This Saharan dust event was marked by an anomalously high dust loading for September (see section S.4), with an AOD > 4 as observed by MODIS *Aqua* and *Terra* (Fig. 11a). To date, this event is the highest dust AOD (~3) ever observed by the DC-8. Figure 14a shows the vertical cross section of aerosol backscatter from HALO and W-/Ka-/Ku-band reflectivity from APR-3 that, when combined with dropsonde profiles in the vicinity of the AEW (Figs. 13d,e), highlights the complex layering of dust, dry air, and convection for this case. HALO observed a geometrically thin but optically thick dust layer with peak AOD mostly confined to 2–3.5 km as it interacted with the developing AEW to the east of the dust event. While most of the dust loading was elevated for this event, some were again observed in the MBL (e.g., 0920–0945 UTC), again underscoring that dust outbreaks emerging from Africa do not always follow the deep, well-mixed conceptual model (Karyampudi et al. 1999). Following an east–west remote sensing leg at 18°N, an in situ leg was then performed at ~2.5 km in the region of peak backscatter observed by HALO at 1040 UTC, followed by sampling down to 0.15 km and then sampling again through the peak aerosol loading located at 2.5 km. Figure 14b shows aerosol particle size distributions observed by CAPS at various altitude ranges and indicates the presence of giant-size particles, with peak concentrations within the 2–3-km range. The small-scale variability in dust vertical distributions and associated optical property and particle size in the vicinity of a developing tropical system observed during RF09 pose a challenge to resolution-limited aerosol models to accurately represent aerosol transport and cloud interaction processes. Therefore, this case provides an excellent case study to test and improve the understanding of downwind impacts of process-level representation as models move toward finer spatiotemporal resolutions.

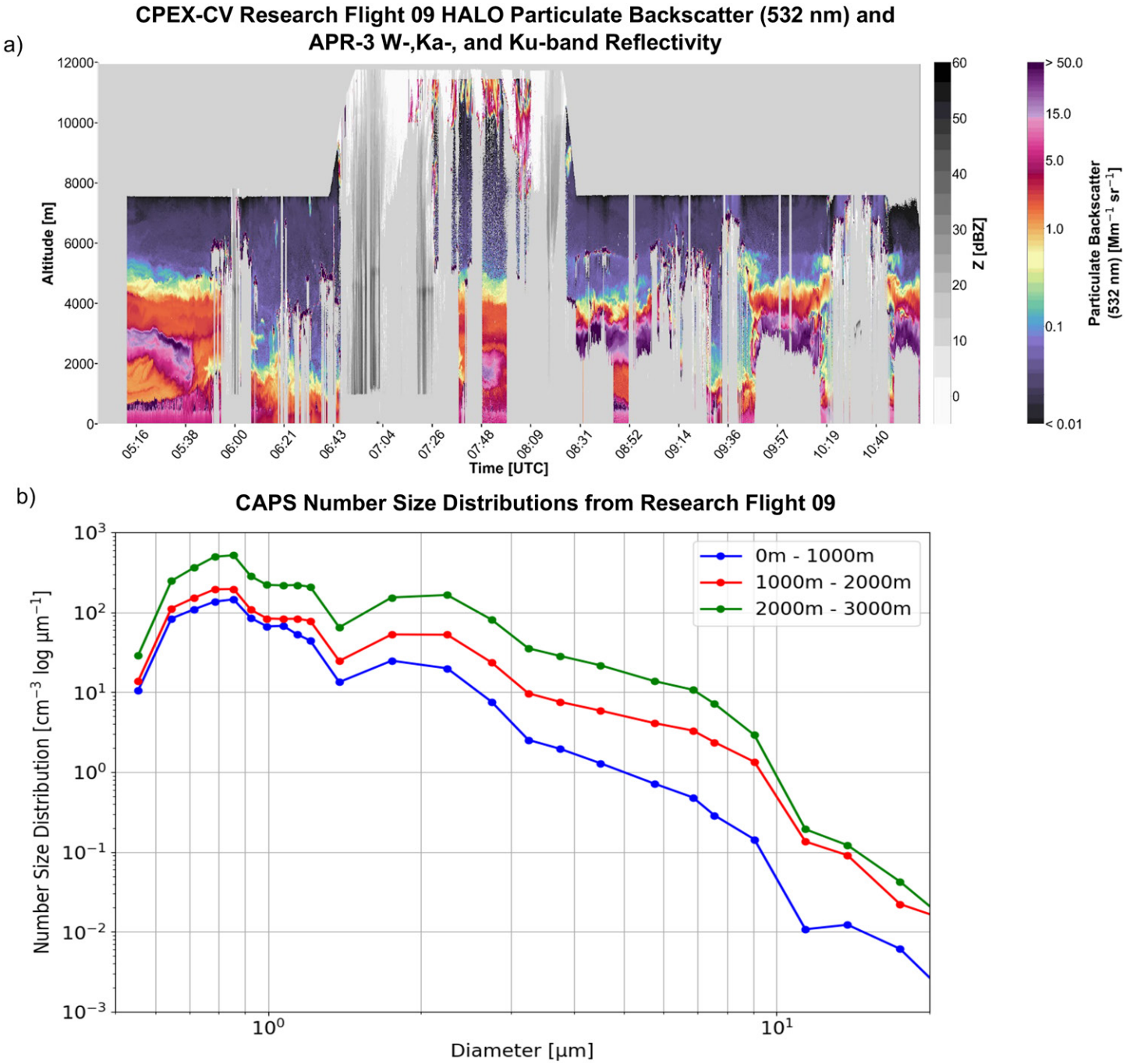

Fig. 14. (a) HALO 532-nm backscatter and APR-3 W/Ka/Ku reflectivity during RF09 on 22 Sep 2022; (b) CAPS average particle size distribution from 1105 to 1300 UTC at various altitude ranges when DC-8 penetrating the dust plume.

On the following day, despite the indication of adverse interactions from the dust-laden SAL, this AEW developed into TS Hermine and was sampled by the DC-8 during RF10 as the SAL wrapped around the storm from the west and the south. Unfortunately, during RF10, an air traffic control strike limited sampling of the eastern side of the storm, and in subsequent days, Hermine dissipated as it tracked north. Combined data from the CPEX-CV payload provide an opportunity to explore potential mechanisms that sustained the observed MCS once it reached the coast and the effects of the dusty SAL on the genesis and development of TS Hermine on back-to-back research flights.

i. Data assimilation. In the postdeployment phase of CPEX-CV, significant strides have been made to understand the contributions of CPEX-CV and available satellite data to the numerical simulation and forecasting of tropical storms and MCSs in September 2022.

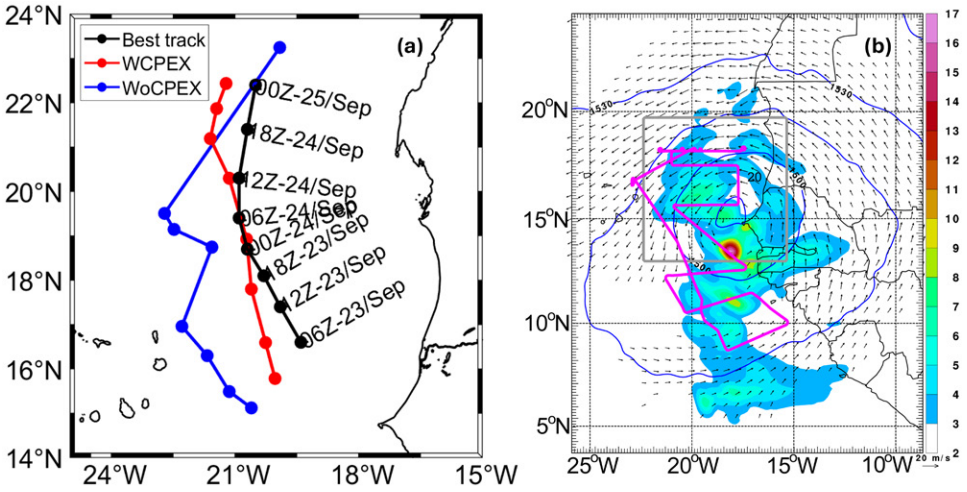

Fig. 15. (a) TS Hermine tracks during 0600 UTC 23–0000 UTC 25 Sep 2022 from the observation (NOAA NHC best track data; the black line) and 42-h forecasts with (WCPEX; the red line) and without (WoCPEX; the blue line) the assimilation of CPEX-CV RF09 data in the UC Davis WRF dust model. The initial conditions for WCPEX and WoCPEX were from the 40-member ensemble analysis means, which cycle forecast–data assimilation 6 hourly for two and a half days. The modeled tracks were located with the pressure minimum centroid at 2 km above sea level. (b) COAMPS adjoint sensitivity was valid at the initial time of 1200 UTC 22 Sep. Vertically integrated sensitivity of the 12–24-h forecast zonal wind component to the initial zonal wind component is shown in the color fill. The response function extends from 850 to 300 hPa and horizontally over the gray box. The initial 850-hPa heights (blue contours) and wind vectors (greater than 5 m s^{-1}) are shown. The flight track is shown in the magenta. The sensitivity shown is scaled by $1 \times 10^{14}/(dx \times dy \times dz)$.

CPEX-CV has provided an unparalleled avenue to assess the observational effects of data assimilation on numerical simulations and prediction of MCSs, tropical storms, and their environments in the tropical East Atlantic, with RF09 and RF10 providing excellent examples. After becoming a TS at 1800 UTC 23 September, Hermine moved northward and quickly weakened into a tropical depression at 1200 UTC 24 September as it encountered stronger shear and cooler sea surface temperatures. CPEX-CV observations have been shown to enhance the predictive accuracy of the TS Hermine track (Fig. 15a), mainly due to the bias correction in the zonal flow. Assimilated CPEX-CV data include DAWN winds, HALO moisture, dropsondes, and radiosondes, along with conventional and satellite data from NOAA NCEP GDAS. NRL's COAMPS adjoint sensitivity analysis for TS Hermine is shown in Fig. 15b, valid at the initial time of 1200 UTC 22 September, highlighting the sensitive regions that influence the track of TS Hermine, particularly the cross-track zonal wind component. The DC-8 flew through the most sensitive region identified by the adjoint analysis (Fig. 15b), and simulation results corroborate the substantial observational impact on track forecast from data assimilation in the data-sparse tropical East Atlantic (Fig. 15a). Additionally, as part of postfield research phases, these real-time forecasts underwent validation against field observational data and are thus further shaping model evaluation, improvement, and data assimilation efforts.

4. Professional development

Involvement of students in field campaigns has a long history in atmospheric science, providing scientific training and networking opportunities (e.g., Hallett et al. 1990; Stith and Rogers 2004; Kristovich et al. 2017; Rasmussen et al. 2021; Swap 2021). Indeed, many of the Principle Investigators (PIs) in CPEX-CV were drawn to pursue a career in this field owing to student participation in field campaigns. In addition to the science described above, a major goal of CPEX-CV and a priority of CPEX-CV leadership were to provide professional development opportunities for students and early career scientists and to do so in a welcoming and

inclusive environment. A quarter of all participants in the field were students and postdocs, rotating through the series of necessary roles to ensure a successful campaign. Our team is especially proud of the leadership opportunities provided to students and early career scientists, including serving as forecast leads and flight scientists.

We followed recently articulated recommendations for creating a positive community to promote cultural change in atmospheric science fieldwork (Fischer et al. 2021). Before the field phase, the CPEX-CV team members—across all career stages and roles within the campaign—codeveloped a code of conduct and required all team members to sign off on it before the campaign. An external facilitator led the team for an in-person bystander intervention training along with team-building exercises to establish a sense of community and trust. Another benefit of team building was that team members became aware of the scientific goals of others, which promoted opportunities for PIs, postdocs, and students across all science areas of the campaign to rotate through as mission and flight scientists throughout the field phase. These precampaign and in-field activities were followed up by select postcampaign interviews on the effects of team building and training activities on participants' experiences in the field. The facilitator developed and briefed anonymized summary assessments to NASA Headquarters management throughout their involvement.

5. Summary

This overview of CPEX-CV highlights a subset of the 13 research flights that targeted process-level interactions between AEWs, MCSs, SAL, WAM, Saharan dust outbreaks, and MBL evolution in the tropical East Atlantic during September 2022. More specifically, the flights sampled various stages of the convective life cycle, offshore convection development, scales of convection in the vicinity of dust, dust outbreaks of varying loadings and vertical distribution, and weak and strong AEWs, including some that went on to form TCs. Sampling of this complex, coupled system in the tropical East Atlantic was possible through the synergistic airborne remote sensing and in situ instrumentation deployed on the NASA DC-8 that permitted profiling of the atmosphere, complementing spatiotemporal gaps in space-based observations in a region with high observation impact. Preliminary analysis has already shown the positive effect of CPEX-CV observations on mesoscale forecasting capabilities in this data-sparse region (e.g., Fig. 15). Ongoing research by the community is focused on unraveling key processes that contributed to the observed findings during CPEX-CV to improve how these underlying processes are characterized in global and mesoscale models. The eventual goal is to improve aerosol, convective life cycle, and transport processes in global and mesoscale models. Additionally, CPEX-CV provided satellite validation of ESA's Aeolus spaceborne wind lidar with collaboration from ground-based ASKOS and airborne CAVA-AW partners within the framework of JATAC 2022. This collaboration underscores the value of advanced planning to leverage cross agency and international assets to enhance coverage and sampling, thereby augmenting information content and sampling in future field campaign efforts.

We finally emphasize the value of providing team-building and professional development opportunities to the team as part of preparations before going into the field. This effort helped establish a collaborative atmosphere among team members from all career stages and understand the diverse CPEX-CV science objectives ahead of the campaign. While deployed, the team was equipped with support tools to handle the rigors of fieldwork, especially within such a large team, and emerge cohesive to tackle the science objectives of CPEX-CV.

Acknowledgments. We would like to acknowledge the support of the NASA Earth Science Project Office (ESPO) and the NASA DC-8 team provided during the preparation, deployment, and postdeployment phases of the campaign. We thank Dr. Hal Maring for serving as the CPEX-CV Program Scientist and for helpful comments on the manuscript. We would like to additionally thank the Office

of Naval Research (ONR) Code 322 for their contributions that enhanced the CPEX-CV deployment. We thank ESA, ASKOS, and UNG for in-field and postdeployment support that enabled continued NASA-ESA collaboration in field campaigns that took place in the tropical North Atlantic. We thank Ben Rodenkirch for his help to homogenize figures from the various CPEX-CV flights. Finally, we thank the numerous early career CPEX-CV participants who contributed to the success of the deployment in various roles. Support for the CPEX-CV deployment was provided by the NASA Weather Program (NNH19ZDA001N-ATDM) and ONR. Part of the research was carried out at the Jet Propulsion Laboratory, California Institute of Technology, under a contract with the National Aeronautics and Space Administration (80NM0018D0004). ASKOS campaign and data curation were funded by the ASKOS ESA project (Contract 4000131861/20/NL/IA); the D-TECT ERC-CoG (Agreement 725698); BMWi (Grant 50EE1721C); BMBF (Grant 01LK1603A); the PANGEA4 CalVal project (Grant Agreement 101079201) funded by the European Union; and the HFRI Research Projects to support postdoctoral researchers (project acronym: REVEAL; Project 07222). UNG funding for CAVA-AW was through ESA CAVA-AW (Contract 4000131931/20/NL/FF/an), ARRS/ARIS (Programs P1-0385 and I0-0033).

Data availability statement. The CPEX-CV data DOI is available at http://doi.org/10.5067/CPEXCV/DATA101 (Zawislak et al. 2022). CPEX-CV data can be accessed through the NASA Global Hydrometeorology Resource Center (GHRC) Distributed Active Archive Center (DAAC) at https://ghrc.nsstc.nasa.gov/home/field-campaigns/cpex-cv, the NASA Atmospheric Science Data Center (ASDC) at https://asdc.larc.nasa.gov/project/CPEX-CV, and the NASA LaRC Suborbital Science Data for Atmospheric Composition at https://www-air.larc.nasa.gov/missions/cpex-cv/index.html. Satellite data used during CPEX-CV are available through the NASA JPL portal at https://cpex-aw.jpl.nasa.gov/ and the University of Wisconsin geoworldview site (https://geoworldview.ssec.wisc.edu/). The ASKOS campaign data are publicly available via the ESA Validation Data Center (EVDC) portal at https://evdc.esa.int/publications/askos-campaign-dataset/. CAVA-AW data are available at https://evdc-review.skytek.com/publications/jataccava-aw-aeolus-calval-airborne-campaign-dataset/. ERA5 data were accessed via NCAR Research Data Archive (https://rda.ucar.edu/datasets/ds633.0/) through the Computational and Information Systems Laboratory (CISL). MODIS *Terra* and *Aqua* aerosol optical depth can be accessed from https://ladsweb.modaps.eosdis.nasa.gov/missions-and-measurements/science-domain/aerosol/. GPM IMERG data may be accessed at https://disc.gsfc.nasa.gov/. MSG *Meteosat-11* data can be accessed via https://data.eumetsat.int/. The TAMS MCS tracker can be obtained from Núñez Ocasio's GitHub and the TAMS documentation page (https://tams.readthedocs.io/en/latest/). The AEW tracker and data can be obtained from Lawton's tracker contribution page (https://doi.org/10.17605/OSF.IO/J4HPQ). The input data for TAMS are the infrared channel from MSG.

In memoriam

We dedicate this manuscript to two people critical to the success of CPEX-CV who unfortunately passed away too soon: Claire Robinson and Dr. Gail Skofronick-Jackson (Fig. SB1). Claire was critical to the success of CPEX-CV, often operating multiple instruments at the same time on all flights, and was key to the success of numerous past NASA field campaigns. Her passing is a huge loss for the atmospheric science community, and her presence in the field will be greatly missed.

Dr. Gail Skofronick-Jackson (Fig. SB2) was the NASA official responsible for establishing the CPEX-AW mission in 2021. Following her tragic passing in 2021, the mission resumed as CPEX-CV based out of Cabo Verde, as originally intended by Gail, in 2022. CPEX-CV honored Gail's legacy by dedicating all dropsonde waypoints in her name during RF02 on 7 September 2022.

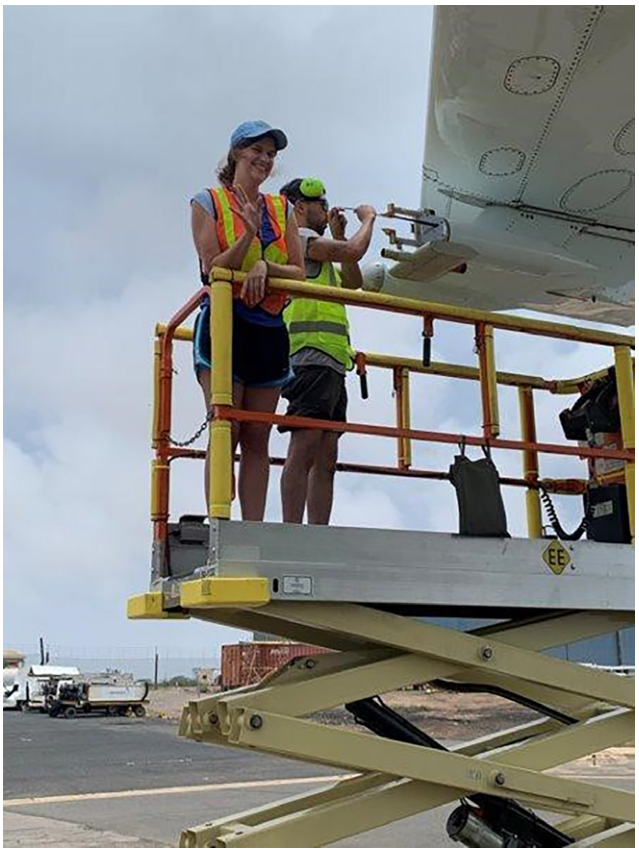

Fig. SB1. The late Claire Robinson integrating the CAPS probe on the DC-8 in Cabo Verde for CPEX-CV.

Fig. SB2. The late Dr. Gail Skofronick-Jackson, who conceived the CPEX-AW deployment planned for Cabo Verde in 2020 before postponing and relocating to Saint Croix, U.S. Virgin Islands, in 2021.

References

Baumgardner, D., H. Jonsson, W. Dawson, D. O'Connor, and R. Newton, 2001: The cloud, aerosol and precipitation spectrometer: A new instrument for cloud investigations. *Atmos. Res.*, **59–60**, 251–264, https://doi.org/10.1016/S0169-8095(01)00119-3.

Bedka, K. M., and Coauthors, 2021: Airborne lidar observations of wind, water vapor, and aerosol profiles during the NASA Aeolus calibration and validation (Cal/Val) test flight campaign. *Atmos. Meas. Tech.*, **14**, 4305–4334, https://doi.org/10.5194/amt-14-4305-2021.

Biasutti, M., S. E. Yuter, C. D. Burleyson, and A. H. Sobel, 2012: Very high resolution rainfall patterns measured by TRMM precipitation radar: Seasonal and diurnal cycles. *Climate Dyn.*, **39**, 239–258, https://doi.org/10.1007/s00382-011-1146-6.

Bleck, R., 2002: An oceanic general circulation model framed in hybrid isopycnic-Cartesian coordinates. *Ocean Modell.*, **4**, 55–88, https://doi.org/10.1016/S1463-5003(01)00012-9.

Braun, S. A., 2010: Reevaluating the role of the Saharan air layer in Atlantic tropical cyclogenesis and evolution. *Mon. Wea. Rev.*, **138**, 2007–2037, https://doi.org/10.1175/2009MWR3135.1.

——, and Coauthors, 2013: NASA's Genesis and Rapid Intensification Processes (GRIP) field experiment. *Bull. Amer. Meteor. Soc.*, **94**, 345–363, https://doi.org/10.1175/BAMS-D-11-00232.1.

Brown, S. T., B. Lambrigtsen, R. F. Denning, T. Gaier, P. Kangaslahti, B. H. Lim, J. M. Tanabe, and A. B. Tanner, 2011: The High-Altitude MMIC Sounding Radiometer for the Global Hawk unmanned aerial vehicle: Instrument description and performance. *IEEE Trans. Geosci. Remote Sens.*, **49**, 3291–3301, https://doi.org/10.1109/TGRS.2011.2125973.

Burpee, R. W., 1972: The origin and structure of easterly waves in the lower troposphere of North Africa. *J. Atmos. Sci.*, **29**, 77–90, https://doi.org/10.1175/1520-0469(1972)029<0077:TOASOE>2.0.CO;2.

——, 1974: Characteristics of North African easterly waves during the summers of 1968 and 1969. *J. Atmos. Sci.*, **31**, 1556–1570, https://doi.org/10.1175/1520-0469(1974)031<1556:CONAEW>2.0.CO;2.

Carroll, B. J., A. R. Nehrir, S. A. Kooi, J. E. Collins, R. A. Barton-Grimley, A. Notari, D. B. Harper, and J. Lee, 2022: Differential absorption lidar measurements of water vapor by the High Altitude Lidar Observatory (HALO): Retrieval framework and first results. *Atmos. Meas. Tech.*, **15**, 605–626, https://doi.org/10.5194/amt-15-605-2022.

Chen, S.-H., S.-H. Wang, and M. Waylonis, 2010: Modification of Saharan air layer and environmental shear over the eastern Atlantic Ocean by dust-radiation effects. *J. Geophys. Res.*, **115**, D21202, https://doi.org/10.1029/2010JD014158.

Chen, S. H., Y. C. Liu, T. R. Nathan, C. Davis, R. Torn, N. Sowa, C. T. Cheng, and J. P. Chen, 2015: Modeling the effects of dust-radiative forcing on the movement of Hurricane Helene (2006). *Quart. J. Roy. Meteor. Soc.*, **141**, 2563–2570, https://doi.org/10.1002/qj.2542.

Chen, S. S., and M. Curcic, 2016: Ocean surface waves in Hurricane Ike (2008) and Superstorm Sandy (2012): Coupled model predictions and observations. *Ocean Modell.*, **103**, 161–176, https://doi.org/10.1016/j.ocemod.2015.08.005.

Cifelli, R., T. Lang, S. A. Rutledge, N. Guy, E. J. Zipser, J. Zawislak, and R. Holzworth, 2010: Characteristics of an African Easterly Wave Observed during NAMMA. *J. Atmos. Sci.*, **67**, 3–25, https://doi.org/10.1175/2009JAS3141.1.

Colarco, P., A. da Silva, M. Chin, and T. Diehl, 2010: Online simulations of global aerosol distributions in the NASA GEOS-4 model and comparisons to satellite and ground-based aerosol optical depth. *J. Geophys. Res.*, **115**, D14207, https://doi.org/10.1029/2009JD012820.

Colarco, P. R., and Coauthors, 2003: Saharan dust transport to the Caribbean during PRIDE: 2. Transport, vertical profiles, and deposition in simulations of in situ and remote sensing observations. *J. Geophys. Res.*, **108**, 8590, https://doi.org/10.1029/2002JD002659.

——, E. P. Nowottnick, C. A. Randles, B. Yi, P. Yang, K. M. Kim, J. A. Smith, and C. G. Bardeen, 2014: Impact of radiatively interactive dust aerosols in the NASA GEOS-5 climate model: Sensitivity to dust particle shape and refractive index. *J. Geophys. Res. Atmos.*, **119**, 753–786, https://doi.org/10.1002/2013JD020046.

Cook, K. H., 1999: Generation of the African easterly jet and its role in determining West African precipitation. *J. Climate*, **12**, 1165–1184, https://doi.org/10.1175/1520-0442(1999)012<1165:GOTAEJ>2.0.CO;2.

DeLonge, M. S., J. D. Fuentes, S. Chan, P. A. Kucera, E. Joseph, A. T. Gaye, and B. Daouda, 2010: Attributes of mesoscale convective systems at the land-ocean transition in Senegal during NASA African Monsoon Multidisciplinary Analyses 2006. *J. Geophys. Res.*, **115**, D10213, https://doi.org/10.1029/2009JD012518.

Denjean, C., and Coauthors, 2016: Size distribution and optical properties of mineral dust aerosols transported in the western Mediterranean. *Atmos. Chem. Phys.*, **16**, 1081–1104, https://doi.org/10.5194/acp-16-1081-2016.

Donelan, M. A., M. Curcic, I. S. Chen, and A. K. Magnusson, 2012: Modeling waves and wind stress. *J. Geophys. Res.*, **117**, C00J23, https://doi.org/10.1029/2011JC007787.

Doyle, J. D., C. A. Reynolds, C. Amerault, and J. Moskaitis, 2012: Adjoint sensitivity and predictability of tropical cyclogenesis. *J. Atmos. Sci.*, **69**, 3535–3557, https://doi.org/10.1175/JAS-D-12-0110.1.

——, ——, and ——, 2019: Adjoint sensitivity analysis of high-impact extratropical cyclones. *Mon. Wea. Rev.*, **147**, 4511–4532, https://doi.org/10.1175/MWR-D-19-0055.1.

Dunion, J. P., and C. S. Velden, 2004: The impact of the Saharan air layer on Atlantic tropical cyclone activity. *Bull. Amer. Meteor. Soc.*, **85**, 353–366, https://doi.org/10.1175/BAMS-85-3-353.

Durden, S. L., S. Tanelli, and E. Im, 2012: Recent observations of clouds and precipitation by the airborne precipitation radar 2nd generation in support of the GPM and ACE missions. *Proc. SPIE*, **8523**, 85230M, https://doi.org/10.1117/12.977574.

Emanuel, K. A., 1989: The finite-amplitude nature of tropical cyclogenesis. *J. Atmos. Sci.*, **46**, 3431–3456, https://doi.org/10.1175/1520-0469(1989)046<3431:TFANOT>2.0.CO;2.

Evan, A. T., and S. Mukhopadhyay, 2010: African dust over the northern tropical Atlantic: 1955–2008. *J. Appl. Meteor. Climatol.*, **49**, 2213–2229, https://doi.org/10.1175/2010JAMC2485.1.

——, J. Dunion, J. A. Foley, A. K. Heidinger, and C. S. Velden, 2006: New evidence for a relationship between Atlantic tropical cyclone activity and African dust outbreaks. *Geophys. Res. Lett.*, **33**, L19813, https://doi.org/10.1029/2006GL026408.

Fang, J., and Y. Du, 2022: A global survey of diurnal offshore propagation of rainfall. *Nat. Commun.*, **13**, 7437, https://doi.org/10.1038/s41467-022-34842-0.

Fehr, T., and Coauthors, 2023: The Joint Aeolus Tropical Atlantic Campaign 2021/2022 Overview–Atmospheric Science and Satellite Validation in the Tropics. Vienna, Austria, European Geophysical Union, EGU23-7249, https://doi.org/10.5194/egusphere-egu23-7249.

Fischer, E. V., and Coauthors, 2021: Leveraging field-campaign networks to identify sexual harassment in atmospheric science and pilot promising interventions. *Bull. Amer. Meteor. Soc.*, **102**, E2137–E2150, https://doi.org/10.1175/BAMS-D-19-0341.1.

Ginoux, P., J. M. Prospero, T. E. Gill, N. C. Hsu, and M. Zhao, 2012: Global-scale attribution of anthropogenic and natural dust sources and their emission rates based on MODIS Deep Blue aerosol products. *Rev. Geophys.*, **50**, RG3005, https://doi.org/10.1029/2012RG000388.

Greco, S., G. D. Emmitt, A. DuVivier, K. Hines, and M. Kavaya, 2020a: Polar winds: Airborne Doppler wind lidar missions in the Arctic for atmospheric observations and numerical model comparisons. *Atmosphere*, **11**, 1141, https://doi.org/10.3390/atmos11111141.

——, ——, M. Garstang, and M. Kavaya, 2020b: Doppler Aerosol WiNd (DAWN) lidar during CPEX 2017: Instrument performance and data utility. *Remote Sens.*, **12**, 2951, https://doi.org/10.3390/rs12182951.

Grossman, R. L., and D. R. Durran, 1984: Interaction of low-level flow with the Western Ghat Mountains and offshore convection in the summer monsoon.

Mon. Wea. Rev., **112**, 652–672, https://doi.org/10.1175/1520-0493(1984)112<0652:IOLLFW>2.0.CO;2.

Gutleben, M., S. Groß, M. Wirth, C. Emde, and B. Mayer, 2019: Impacts of water vapor on Saharan air layer radiative heating. *Geophys. Res. Lett.*, **46**, 14 854–14 862, https://doi.org/10.1029/2019GL085344.

Hallett, J., J. G. Hudson, and A. Schanot, 1990: Student training in facilities in atmospheric science: A teaching experiment. *Bull. Amer. Meteor. Soc.*, **71**, 1637–1641, https://doi.org/10.1175/1520-0477-71.11.1637.

Hamilton, H. L., G. S. Young, J. L. Evans, J. D. Fuentes, and K. M. Núñez Ocasio, 2017: The relationship between the Guinea Highlands and the West African offshore rainfall maximum. *Geophys. Res. Lett.*, **44**, 1158–1166, https://doi.org/10.1002/2016GL071170.

Harrah, S. D., and Coauthors, 2019: Radar detection of high concentrations of ice particles – Methodology and preliminary flight test results. NASA/TP-2019-22043, 42 pp., https://ntrs.nasa.gov/api/citations/20200000699/downloads/20200000699.pdf.

Hock, T. F., and J. L. Franklin, 1999: The NCAR GPS dropwindsonde. *Bull. Amer. Meteor. Soc.*, **80**, 407–420, https://doi.org/10.1175/1520-0477(1999)080<0407:TNGD>2.0.CO;2.

Houze, R. A., Jr., 1977: Structure and dynamics of a tropical squall-line system. *Mon. Wea. Rev.*, **105**, 1540–1567, https://doi.org/10.1175/1520-0493(1977)105<1540:SADOAT>2.0.CO;2.

——Jr., and A. K. Betts, 1981: Convection in GATE. *Rev. Geophys.*, **19**, 541–576, https://doi.org/10.1029/RG019i004p00541.

Houze, R. A., S. G. Geotis, F. D. Marks, and A. K. West, 1981: Winter monsoon convection in the vicinity of North Borneo. Part I: Structure and time variation of the clouds and precipitation. *Mon. Wea. Rev.*, **109**, 1595–1614, https://doi.org/10.1175/1520-0493(1981)109<1595:WMCITV>2.0.CO;2.

——, K. L. Rasmussen, M. D. Zuluaga, and S. R. Brodzik, 2015: The variable nature of convection in the tropics and subtropics: A legacy of 16 years of the Tropical Rainfall Measuring Mission satellite. *Rev. Geophys.*, **53**, 994–1021, https://doi.org/10.1002/2015RG000488.

Hristova-Veleva, S. M., and Coauthors, 2020: An eye on the storm: Integrating a wealth of data for quickly advancing the physical understanding and forecasting of tropical cyclones. *Bull. Amer. Meteor. Soc.*, **101**, E1718–E1742, https://doi.org/10.1175/BAMS-D-19-0020.1.

Huang, C. C., and Coauthors, 2019: Impacts of dust–radiation versus dust–cloud interactions on the development of a Modeled Mesoscale Convective System over North Africa. *Mon. Wea. Rev.*, **147**, 3301–3326, https://doi.org/10.1175/MWR-D-18-0459.1.

Ismail, S., and Coauthors, 2010: LASE measurements of water vapor, aerosol, and cloud distributions in Saharan air layers and tropical disturbances. *J. Atmos. Sci.*, **67**, 1026–1047, https://doi.org/10.1175/2009JAS3136.1.

Jickells, T. D., and Coauthors, 2005: Global iron connections between desert dust, ocean biogeochemistry, and climate. *Science*, **308**, 67–71, https://doi.org/10.1126/science.1105959.

Karyampudi, V. M., and Coauthors, 1999: Validation of the Saharan dust plume conceptual model using lidar, meteosat, and ECMWF data. *Bull. Amer. Meteor. Soc.*, **80**, 1045–1076, https://doi.org/10.1175/1520-0477(1999)080<1045:VOTSDP>2.0.CO;2.

Kaufman, Y. J., I. Koren, L. A. Remer, D. Rosenfeld, and Y. Rudich, 2005: The effect of smoke, dust, and pollution aerosol on shallow cloud development over the Atlantic Ocean. *Proc. Natl. Acad. Sci. USA*, **102**, 11 207–11 212, https://doi.org/10.1073/pnas.0505191102.

Kavaya, M. J., J. Y. Beyon, G. J. Koch, M. Petros, P. J. Petzar, U. N. Singh, B. C. Trieu, and J. Yu, 2014: The Doppler Aerosol Wind (DAWN) airborne, wind-profiling coherent-detection lidar system: Overview and preliminary flight results. *J. Atmos. Oceanic Technol.*, **31**, 826–842, https://doi.org/10.1175/JTECH-D-12-00274.1.

Kristovich, D. A. R., and Coauthors, 2017: The Ontario winter lake-effect systems field campaign: Scientific and educational adventures to further our knowledge and prediction of lake-effect storms. *Bull. Amer. Meteor. Soc.*, **98**, 315–332, https://doi.org/10.1175/BAMS-D-15-00034.1.

Kuettner, J. P., 1974: General description and central program of GATE. *Bull. Amer. Meteor. Soc.*, **55**, 712–719.

Laing, A. G., and J. M. Fritsch, 1993: Mesoscale convective complexes in Africa. *Mon. Wea. Rev.*, **121**, 2254–2263, https://doi.org/10.1175/1520-0493(1993)121<2254:MCCIA>2.0.CO;2.

Landsea, C. W., G. D. Bell, W. M. Gray, and S. B. Goldenberg, 1998: The extremely active 1995 Atlantic hurricane season: Environmental conditions and verification of seasonal forecasts. *Mon. Wea. Rev.*, **126**, 1174–1193, https://doi.org/10.1175/1520-0493(1998)126<1174:TEAAHS>2.0.CO;2.

Lau, K. M., and K. M. Kim, 2007: Cooling of the Atlantic by Saharan dust. *Geophys. Res. Lett.*, **34**, L23811, https://doi.org/10.1029/2007GL031538.

Lawton, Q. A., S. J. Majumdar, K. Dotterer, C. Thorncroft, and C. J. Schreck, 2022: The influence of convectively coupled Kelvin waves on African easterly waves in a wave-following framework. *Mon. Wea. Rev.*, **150**, 2055–2072, https://doi.org/10.1175/MWR-D-21-0321.1.

Leary, C. A., and R. A. Houze, 1979: The structure and evolution of convection in a tropical cloud cluster. *J. Atmos. Sci.*, **36**, 437–457, https://doi.org/10.1175/1520-0469(1979)036<0437:TSAEOC>2.0.CO;2.

Liu, Z., and Coauthors, 2008: CALIPSO lidar observations of the optical properties of Saharan dust: A case study of long-range transport. *J. Geosphys. Res. Atmos.*, **113**, D07207, https://doi.org/10.1029/2007JD008878.

Mahowald, N., S. Albani, J. F. Kok, S. Engelstaeder, R. Scanza, D. S. Ward, and M. G. Flanner, 2014: The size distribution of desert dust aerosols and its impact on the Earth system. *Aeolian Res.*, **15**, 53–71, https://doi.org/10.1016/j.aeolia.2013.09.002.

Mapes, B. E., T. T. Warner, and M. Xu, 2003: Diurnal patterns of rainfall in northwestern South America. Part III: Diurnal gravity waves and nocturnal convection offshore. *Mon. Wea. Rev.*, **131**, 830–844, https://doi.org/10.1175/1520-0493(2003)131<0830:DPORIN>2.0.CO;2.

Maring, H., D. L. Savoie, M. A. Izaguirre, L. Custals, and J. S. Reid, 2003: Mineral dust aerosol size distribution change during atmospheric transport. *J. Geophys. Res.*, **108**, 8592, https://doi.org/10.1029/2002JD002536.

Marinou, E., and Coauthors, 2023: An overview of the ASKOS campaign in Cabo Verde. *Environ. Sci. Proc.*, **26**, 200, https://doi.org/10.3390/environsciproc2023026200.

Middleton, N. J., P. R. Betzer, and P. A. Bull, 2001: Long-range transport of 'giant' aeolian quartz grains: Linkage with discrete sedimentary sources and implications for protective particle transfer. *Mar. Geol.*, **177**, 411–417, https://doi.org/10.1016/S0025-3227(01)00171-2.

Močnik, G., J. Yus-Díez, M. Bervida, L. Drinovec, B. Žibert, U. Jagodič, and M. Lenarčič, 2023: JATAC/CAVA-AW Aeolus Cal/Val airborne campaign dataset. Accessed 11 November 2023, https://evdc.esa.int/publications/jataccava-aw-aeolus-calval-airborne-campaign-dataset/.

Molteni, F., R. Buizza, T. N. Palmer, and T. Petroliagis, 1996: The ECMWF ensemble prediction system: Methodology and validation. *Quart. J. Roy. Meteor. Soc.*, **122**, 73–119, https://doi.org/10.1002/qj.49712252905.

Nehrir, A. R., and Coauthors, 2017: Emerging technologies and synergies for airborne and space-based measurements of water vapor profiles. *Surv. Geophys.*, **38**, 1445–1482, https://doi.org/10.1007/s10712-017-9448-9.

Nicholls, S. D., and K. I. Mohr, 2010: An analysis of the environments of intense convective systems in West Africa in 2003. *Mon. Wea. Rev.*, **138**, 3721–3739, https://doi.org/10.1175/2010MWR3321.1.

Nowottnick, E. P., P. R. Colarco, S. A. Braun, D. O. Barahona, A. da Silva, D. L. Hlavka, M. J. McGill, and J. R. Spackman, 2018: Dust impacts on the 2012 Hurricane Nadine track during the NASA HS3 field campaign. *J. Atmos. Sci.*, **75**, 2473–2489, https://doi.org/10.1175/JAS-D-17-0237.1.

Núñez Ocasio, K. M., J. L. Evans, and G. S. Young, 2020a: Tracking mesoscale convective systems that are potential candidates for tropical cyclogenesis. *Mon. Wea. Rev.*, **148**, 655–669, https://doi.org/10.1175/MWR-D-19-0070.1.

——, ——, and ——, 2020b: A wave-relative framework analysis of AEW–MCS interactions leading to tropical cyclogenesis. *Mon. Wea. Rev.*, **148**, 4657–4671, https://doi.org/10.1175/MWR-D-20-0152.1.

Ogino, S., M. D. Yamanaka, S. Mori, and J. Matsumoto, 2016: How much is the precipitation amount over the tropical coastal region? *J. Climate*, **29**, 1231–1236, https://doi.org/10.1175/JCLI-D-15-0484.1.

Peatman, S. C., C. E. Birch, J. Schwendike, J. H. Marsham, C. Dearden, S. Webster, R. R. Neely, and A. J. Matthews, 2023: The role of density currents and gravity waves in the offshore propagation of convection over Sumatra. *Mon. Wea. Rev.*, **151**, 1757–1777, https://doi.org/10.1175/MWR-D-22-0322.1.

Persson, A., and F. Grazzini, 2007: User guide to ECMWF forecast products. Meteor. Bull. M3.2, 161 pp., https://www.uio.no/studier/emner/matnat/geofag/nedlagte-emner/GEF4220/v09/undervisningsmateriale/Persson_user_guide.pdf.

Prospero, J. M., 1999: Assessing the impact of advected African dust on air quality and health in the eastern United States. *Hum. Ecol. Risk Assess.*, **5**, 471–479, https://doi.org/10.1080/10807039.1999.10518872.

——, P. Ginoux, O. Torres, S. E. Nicholson, and T. E. Gill, 2002: Environmental characterization of global sources of atmospheric soil dust identified with the Nimbus 7 Total Ozone Mapping Spectrometer (TOMS) absorbing aerosol product. *Rev. Geophys.*, **40**, 1002, https://doi.org/10.1029/2000RG000095.

Pu, B., and Q. Jin, 2021: A record-breaking trans-Atlantic African dust plume associated with atmospheric circulation extremes in June 2020. *Bull. Amer. Meteor. Soc.*, **102**, E1340–E1356, https://doi.org/10.1175/BAMS-D-21-0014.1.

Querol, X., and Coauthors, 2019: Monitoring the impact of desert dust outbreaks for air quality for health studies. *Environ. Int.*, **130**, 104867, https://doi.org/10.1016/j.envint.2019.05.061.

Randles, C. A., P. R. Colarco, and A. Da Silva, 2013: Direct and semi-direct aerosol effects in the NASA GEOS-5 AGCM: Aerosol-climate interactions due to prognostic versus prescribed aerosols. *J. Geophys. Res. Atmos.*, **118**, 149–169, https://doi.org/10.1029/2012JD018388.

Rappaport, E. N., 2014: Fatalities in the United States from Atlantic tropical cyclones: New data and interpretation. *Bull. Amer. Meteor. Soc.*, **95**, 341–346, https://doi.org/10.1175/BAMS-D-12-00074.1.

Rasmussen, K. L., M. A. Burt, A. Rowe, R. Haacker, D. Hence, L. M. Luna, S. W. Nesbitt, and J. Maertens, 2021: Enlightenment strikes! Broadening graduate school training through field campaign participation. *Bull. Amer. Meteor. Soc.*, **102**, E1987–E2001, https://doi.org/10.1175/BAMS-D-20-0062.1.

Reale, O., W. K. Lau, K. Kim, and E. Brin, 2009: Atlantic tropical cyclogenetic processes during SOP-3 NAMMA in the GEOS-5 global data assimilation and forecast system. *J. Atmos. Sci.*, **66**, 3563–3578, https://doi.org/10.1175/2009JAS3123.1.

——, K. M. Lau, and A. da Silva, 2011: Impact of interactive aerosol on the African easterly jet in the NASA GEOS-5 global forecasting system. *Wea. Forecasting*, **26**, 504–519, https://doi.org/10.1175/WAF-D-10-05025.1.

Redelsperger, J. L., and Coauthors, 2006: AMMA, une étude multidisciplinaire de la mousson ouest-africaine. *La Meteorologie*, **54**, 22–32, https://doi.org/10.4267/2042/20098.

Reid, E. A., J. S. Reid, M. M. Meier, M. R. Dunlap, S. S. Cliff, A. Broumas, K. Perry, and H. Maring, 2003: Characterization of African dust transported to Puerto Rico by individual particle and size segregated bulk analysis. *J. Geophys. Res.*, **108**, 8591, https://doi.org/10.1029/2002JD002935.

Reitebuch, O., 2012: The spaceborne wind lidar mission ADM-Aeolus. *Atmospheric Physics*, Springer, 815–827.

Ridout, J. A., 2002: Sensitivity of tropical Pacific convection to dry layers at mid-to upper levels: Simulation and parameterization tests. *J. Atmos. Sci.*, **59**, 3362–3381, https://doi.org/10.1175/1520-0469(2002)059<3362:SOTPCT>2.0.CO;2.

Rosenfeld, D., Y. Rudich, and R. Lahav, 2001: Desert dust suppressing precipitation: A possible desertification feedback loop. *Proc. Natl. Acad. Sci. USA*, **98**, 5975–5980, https://doi.org/10.1073/pnas.101122798.

Rubin, J. I., J. S. Reid, P. Xian, C. M. Selman, and T. F. Eck, 2023: A global evaluation of daily to seasonal aerosol and water vapor relationships using a combination of AERONET and NAAPS reanalysis data. *Atmos. Chem. Phys.*, **23**, 4059–4090, https://doi.org/10.5194/acp-23-4059-2023.

Sadowy, G. A., A. C. Berkun, W. Chun, E. Im, and S. L. Durden, 2003: Development of an advanced airborne precipitation radar. *Microwave J.*, **46**, 84–86.

Schneider, T., T. Bischoff, and G. H. Haug, 2014: Migrations and dynamics of the intertropical convergence zone. *Nature*, **513**, 45–53, https://doi.org/10.1038/nature13636.

Skamarock, W. C., J. B. Klemp, M. G. Duda, L. D. Fowler, S. Park, and T. D. Ringler, 2012: A multiscale nonhydrostatic atmospheric model using centroidal Voronoi Tesselations and C-Grid staggering. *Mon. Wea. Rev.*, **140**, 3090–3105, https://doi.org/10.1175/MWR-D-11-00215.1.

——, and Coauthors, 2019: A description of the Advanced Research WRF version 4.1. NCAR Tech. Note NCAR/TN-556+STR, 162 pp., https://doi.org/10.5065/1dfh-6p97.

Spanu, A., M. Dollner, J. Gasteiger, T. P. Bui, and B. Weinzierl, 2020: Flow-induced errors in airborne in situ measurements of aerosols and clouds. *Atmos. Meas. Tech.*, **13**, 1963–1987, https://doi.org/10.5194/amt-13-1963-2020.

Stith, J., and D. C. Rogers, 2004: Instrument development and education in airborne science. *13th Symp. Education*, Seattle, WA, Amer. Meteor. Soc., 4.12, https://ams.confex.com/ams/84Annual/techprogram/paper_66280.htm.

Swap, R., 2021: Growing our own timber: Perspectives and experiences from the field on training the next generation. AAAS, https://www.sciencediplomacy.org/in-field/2021/growing-our-own-timber-perspectives-and-experiences-field-training-next-generation.

——, M. Garstang, S. Greco, R. Talbot, and P. Kållberg, 1992: Saharan dust in the Amazon basin. *Tellus*, **44B**, 133–149, https://doi.org/10.3402/tellusb.v44i2.15434.

Textor, C., and Coauthors, 2006: Analysis and quantification of the diversities of aerosol life cycles within AeroCom. *Atmos. Chem. Phys.*, **6**, 1777–1813, https://doi.org/10.5194/acp-6-1777-2006.

Thorncroft, C., and K. Hodges, 2001: African easterly wave variability and its relationship to Atlantic tropical cyclone activity. *J. Climate*, **14**, 1166–1179, https://doi.org/10.1175/1520-0442(2001)014<1166:AEWVAI>2.0.CO;2.

Thorncroft, C. D., and B. J. Hoskins, 1994: An idealized study of African easterly waves. I: A linear view. *Quart. J. Roy. Meteor. Soc.*, **120**, 953–982, https://doi.org/10.1002/qj.49712051809.

——, and M. Blackburn, 1999: Maintenance of the African easterly jet. *Quart. J. Roy. Meteor. Soc.*, **125**, 763–786, https://doi.org/10.1002/qj.49712555502.

Torn, R. D., 2010: Ensemble-based sensitivity analysis applied to African easterly waves. *Wea. Forecasting*, **25**, 61–78, https://doi.org/10.1175/2009WAF2222255.1.

Toth, Z., and E. Kalnay, 1997: Ensemble forecasting at NCEP and the breeding method. *Mon. Wea. Rev.*, **125**, 3297–3319, https://doi.org/10.1175/1520-0493(1997)125<3297:EFANAT>2.0.CO;2.

Turk, F. J., S. Hristova-Veleva, S. L. Durden, S. Tanelli, O. Sy, G. D. Emmitt, S. Greco, and S. Q. Zhang, 2020: Joint analysis of convective structure from the APR-2 precipitation radar and the DAWN Doppler wind lidar during the 2017 Convective Processes Experiment (CPEX). *Atmos. Meas. Tech.*, **13**, 4521–4537, https://doi.org/10.5194/amt-13-4521-2020.

Twohy, C. H., and Coauthors, 2009: Saharan dust particles nucleate droplets in eastern Atlantic clouds. *Geophys. Res. Lett.*, **36**, L01807, https://doi.org/10.1029/2008GL035846.

van der Does, M., P. Knippertz, P. Zschenderlein, R. G. Harrison, and J. B. W. Stuut, 2018: The mysterious long-range transport of giant mineral dust particles. *Sci. Adv.*, **4**, eaau2768, https://doi.org/10.1126/sciadv.aau2768.

Wang, S., and A. H. Sobel, 2012: Impact of imposed drying on deep convection in a cloud-resolving model. *J. Geophys. Res.*, **117**, D02112, https://doi.org/10.1029/2011JD016847.

Weinzierl, B., and Coauthors, 2017: The Saharan aerosol long-range transport and aerosol–cloud-interaction experiment: Overview and selected highlights. *Bull. Amer. Meteor. Soc.*, **98**, 1427–1451, https://doi.org/10.1175/BAMS-D-15-00142.1.

Westphal, D. L., O. B. Toon, and T. N. Carlson, 1987: A two-dimensional numerical investigation of the dynamics and microphysics of Saharan dust

storms. *J. Geophs. Res. Atmos.*, **92**, 3027–3049, https://doi.org/10.1029/JD092iD03p03027.

Whitaker, J. S., T. M. Hamill, X. Wei, Y. Song, and Z. Toth, 2008: Ensemble data assimilation with the NCEP Global Forecast System. *Mon. Wea. Rev.*, **136**, 463–482, https://doi.org/10.1175/2007MWR2018.1.

Wick, G. A., and Coauthors, 2020: NOAA's Sensing Hazards with Operational Unmanned Technology (SHOUT) experiment observations and forecast impacts. *Bull. Amer. Meteor. Soc.*, **101**, E968–E987, https://doi.org/10.1175/BAMS-D-18-0257.1.

Wong, S., and A. E. Dessler, 2005: Suppression of deep convection over the tropical North Atlantic by the Saharan air layer. *Geophys. Res. Lett.*, **32**, L09808, https://doi.org/10.1029/2004GL022295.

——, ——, N. M. Mahowald, P. Yang, and Q. Feng, 2009: Maintenance of lower tropospheric temperature inversion in the Saharan air layer by dust and dry anomaly. *J. Climate*, **22**, 5149–5162, https://doi.org/10.1175/2009JCLI2847.1.

Wu, S.-H., N. Sakaeda, E. Martin, R. Rios-Berrios, and J. Russel, 2024: The contribution of mesoscale convective systems to the coastal rainfall maximum over West Africa. *Mon. Wea. Rev.*, **152**, 1787–1802, https://doi.org/10.1175/MWR-D-23-0148.1.

Xian, P., J. S. Reid, J. F. Turk, E. J. Hyer, and D. L. Westphal, 2009: Impact of modeled versus satellite measured tropical precipitation on regional smoke optical thickness in an aerosol transport model. *Geophys. Res. Lett.*, **36**, L16805, https://doi.org/10.1029/2009GL038823.

——, P. J. Klotzbach, J. P. Dunion, M. A. Janiga, J. S. Reid, P. R. Colarco, and Z. Kipling, 2020: Revisiting the relationship between Atlantic dust and tropical cyclone activity using aerosol optical depth reanalyses: 2003–2018. *Atmos. Chem. Phys.*, **20**, 15 357–15 378, https://doi.org/10.5194/acp-20-15357-2020.

Yu, H., and Coauthors, 2021: Observation and modeling of the historic "Godzilla" African dust intrusion into the Caribbean Basin and the southern US in June 2020. *Atmos. Chem. Phys.*, **21**, 12 359–12 383, https://doi.org/10.5194/acp-21-12359-2021.

Yus-Díez, J., G. Močnik, L. Drinovec, M. Bervida Mačak, B. Žibert, U. Jagodič, and M. Lenarčič, 2023: JATAC/CAVA-AW Aeolus Cal/Val airborne campaign dataset. Accessed 11 November 2023, https://evdc.esa.int/publications/jataccava-aw-aeolus-calval-airborne-campaign-dataset/.

Zawislak, J., and E. J. Zipser, 2010: Observations of seven African easterly waves in the East Atlantic during 2006. *J. Atmos. Sci.*, **67**, 26–43, https://doi.org/10.1175/2009JAS3118.1.

——, E. Nowottnick, and A. Nehrir, 2022: Convective Processes Experiment – Cabo Verde (CPEX-CV) Field Campaign Collection. NASA EOSDIS Global Hydrometeorology Resource Center Distributed Active Archive Center, accessed 1 July 2023, https://doi.org/10.5067/CPEXCV/DATA101.

Zhang, C., J. M. Wallace, R. A. Houze, E. J. Zipser, and K. A. Emanuel, 2022: Relocation of GATE from the Pacific to the Atlantic. *Bull. Amer. Meteor. Soc.*, **103**, E1991–E1999, https://doi.org/10.1175/BAMS-D-21-0151.1.

Zhu, A., V. Ramanathan, F. Li, and D. Kim, 2007: Dust plumes over the Pacific, Indian, and Atlantic oceans: Climatology and radiative impact. *J. Geophys. Res.*, **112**, D16208, https://doi.org/10.1029/2007JD008427.

Zipser, E. J., 1977: Mesoscale and convective–Scale downdrafts as distinct components of squall-line structure. *Mon. Wea. Rev.*, **105**, 1568–1589, https://doi.org/10.1175/1520-0493(1977)105<1568:MACDAD>2.0.CO;2.

——, 1994: Deep cumulonimbus cloud systems in the tropics with and without lightning. *Mon. Wea. Rev.*, **122**, 1837–1851, https://doi.org/10.1175/1520-0493(1994)122<1837:DCCSIT>2.0.CO;2.

——, and Coauthors, 2009: The Saharan air layer and the fate of African easterly waves—NASA's AMMA field study of tropical cyclogenesis. *Bull. Amer. Meteor. Soc.*, **90**, 1137–1156, https://doi.org/10.1175/2009BAMS2728.1.